

# Monte Carlo Simulations of Interfaces in Polymer Blends

Marcus Müller and Friederike Schmid

*Institut für Physik, Universität Mainz, D-55099 Mainz, FRG*

**Abstract.** We review recent simulation studies of interfaces between immiscible homopolymer phases. Special emphasis is given to the presentation of efficient simulation techniques and powerful methods of data analysis, such as the analysis of capillary wave spectra. Possible reasons for polymer incompatibility and ways to relate model dependent interaction parameters to an effective Flory Huggins parameter  $\chi$  are discussed. Various interfaces are then considered and characterised with respect to their microscopic structure and thermodynamic properties. In particular, interfaces between homopolymers of equal or disparate stiffness are studied, interfaces containing diblock copolymers, and interfaces confined in thin films. The results are related to the phase behaviour of ternary homopolymer/copolymer systems, and to wetting transitions in thin films.

## 1 Introduction

Blending chemically different polymers is a cheap and relatively straightforward way of creating new materials, and polymeric alloys are therefore industrially and technologically omnipresent. Prominent examples are, *e.g.*, rubber toughened plastics. Their widespread use notwithstanding, polymer mixtures are seldom homogeneous at temperatures of practical interest. Any slight incompatibility of the monomers, as is usually present between different organic molecules, is amplified by the number of monomers in the macromolecule, and cannot be balanced by the entropy of mixing for typical molecular weights [1]. On a mesoscopic scale, such materials consist of numerous microdroplets of one phase, which are finely dispersed in the other phase. The material properties thus depend sensitively on the structure and the properties of the interfaces between different phases. Correlations between interfacial and bulk properties are present on various length scales. On the one hand, the local interfacial structure – the conformation of polymers, the interfacial width, which is closely related to the number of entanglements between polymers of

different type, enrichment of chain ends or solvent at the interface etc – has a fundamental influence on the mechanical stability of the alloy. On the other hand, the morphology of the blend at given conditions of preparation (*e.g.*, given stirring rate during mechanical mixing) is basically determined by the interfacial tension: An old theoretical argument due to Taylor[2] balances the viscous stress (caused by stirring) and the interfacial tension, and predicts that the droplet size should be directly proportional to the latter. This law is indeed found experimentally[3].

A huge number of interesting questions are connected with the general subject of polymer interfaces. For example, interfacial properties can be tailored by adding a small amount of a third substance to the blend[4]. In particular, copolymeric surfactants containing both types of monomers are often used as effective compatibiliser. Their effect on the morphology of the blend is twofold. First, they reduce directly the interfacial tension: Being compatible with both components, they aggregate at interfaces, thereby reducing the number of direct contacts between homopolymers of different type[5]. Second, recent experimental[6] and theoretical[7] studies indicate that their presence at the droplet surface prevents the coalescence of the droplets brought into collision in the course of mixing. The effect can be related to the two-dimensional compression modulus of the copolymer film[7]. Since droplets can break up, but do not merge any more, one obtains a particularly fine dispersion. In addition, copolymers improve the mechanical properties of interfaces. The interfacial width increases, and likewise the number of entanglements, they adhesive attraction and the fracture toughness[8]. At high enough copolymer concentrations, additional copolymer rich phases emerge which display a variety of structures ordered on a mesoscopic scale[9, 10, 11, 12]. These mesoscopically structured materials promise to possess unique and useful materials properties[10, 13, 14].

Another complex of important problems refers to confined interfaces, *i.e.*, interfaces interacting with one or two surfaces. The presence of a surface influences the interface on all length scales – the local structure is affected as well as long wavelength fluctuations of the interface position. Depending on the interactions of the surface with the different components of the blend, the interface may bind or unbind, giving rise to a whole diversity of wetting phenomena[15, 16, 17].

From the point of view of basic science, inhomogeneous polymer systems are interesting because of the different length scales involved (polymer gyration radius vs. monomer size), and because of the additional conformational degrees of freedom of polymers as opposed to smaller molecules. Interestingly, these apparent complications have partly the effect of simplifying the physics: Since polymers interact with so many other polymers, microscopic details of the chemical structure of monomers wash out to a large extent, and can be absorbed quite successfully into a few number of effective parameters. Furthermore, the effective interaction range – roughly the polymer gyration

radius – is very large, and the region in which critical concentration fluctuations become important is extremely small as a consequence (Ginzburg criterion, see Ref. [18]). Polymer blends are thus unusually well described by mean field type theories.

On the other hand, the treatment on the mean field level in itself is already very involved, especially if one attempts to account for local correlations, and is interested in local structures. A number of mean field type approaches have been established in the past years, which differ by level of coarse-graining and by the type of questions they address. Among these, we quote Landau-Ginzburg [19, 20] and scaling approaches[1], which coarse-grain over the microscopic and to some extent even over the chain conformational structure; Self-consistent field theories[21, 22, 23, 24] and density functional theories [25], which treat chains as random walks in a mean field environment, mostly ignoring the monomer structure and local chain correlations; lattice-based theories such as the famous Flory-Huggins theory[26, 27] and subsequent more refined extensions (e.g, [28, 29, 30]); and finally Schweizer’s and Curro’s P-RISM theory[31], which incorporates the local liquid structure into a theory of polymer melts, using concepts from integral equation theories for simple liquids. The highly coarse-grained theories have the advantage of relative simplicity, thus allowing in many cases for an analytical treatment. However, the information they can provide on local structure properties is, *a priori*, very limited. Furthermore, they require a number of “effective” parameters as input, which cannot be determined from microscopic parameters within the theory. On the other hand, the more microscopic details are incorporated into a mean field theory, the more involved the treatment gets, and the more additional approximations have to be made in order to make it tractable at all. At the lowest level of coarse-graining, for example, the P-RISM equations totally neglect chain end effects, but their truly self-consistent solution in a one component melt nonetheless requires a series of single chain Monte Carlo simulations[31, 32].

The universal aspect of the physics of polymeric alloys, and the close relationship between the local structure of interfaces and the global material properties, make them particularly suited for computer simulations[33, 34]. These provide simultaneously a detailed microscopic picture of the interfacial structure, and information on the thermodynamics of the interfaces. When compared to experiments, they serve as a test of the microscopic model which has been used. When compared to theories, they serve as a test of the theory, within a well-defined microscopic model. In addition, they may provide structural information which may not yet be accessible experimentally or theoretically. They can thus contribute substantially towards a deeper understanding of the connections between the microscopic parameters, the microscopic structure and the macroscopic properties of a material.

Obviously, there are limitations. With the present computational resources, full calculations of polymer melts in atomistic detail are currently

far beyond reach. It is thus necessary to take again advantage of the universality idea[1, 27, 35], and represent real polymeric system by idealised polymer models. In this spirit, a number of chemical monomer units are mapped onto one effective monomer with a much simpler structure. Even within such a simplified model, only melts of polymers of rather modest chain lengths can currently be equilibrated and subsequently studied. Depending on the questions that one wishes to study, models of different levels of idealisation have to be chosen. The careful choice of a suitable model is thus crucial for the success of an investigation. We will discuss this important point in more detail in Sec.3. The reader interested in a general overview over the use of computer simulations in polymer science is referred to, *e.g.*, the set of excellent reviews in Ref.[33].

In this contribution, we will review some recent simulation studies of polymer interfaces in polymer blends. We shall restrict ourselves to interfaces at thermodynamical equilibrium, and to studies of static properties. Our survey will focus on the insight that simulation studies can provide into the local structure of interfaces, and the implications for the global thermodynamics of the systems. We will start with the closely related issue of the general relationship between local correlations and thermodynamic miscibility in binary blends. Then, we will discuss interphase boundaries in binary homopolymer blends. The effect of adding diblock copolymers on the interface and on the phase diagram is considered. Finally the behaviour in a thin film is examined, with special emphasis on the effect of the interfacial fluctuations on the measured profiles.

## 2 Polymer incompatibility and Flory Huggins parameter

We begin with a discussion of polymer incompatibility: Immiscibility in polymer blends can be caused by several factors. First, one has usually a direct relative repulsion between monomers of different type. In nonpolar molecules, for example, the van der Waals attraction between monomers  $i$  and  $j$  is proportional to the product of their polarisabilities  $\alpha_i\alpha_j$ . Thus the interaction between unlike monomers is smaller than the arithmetic mean of the interactions between like monomers – which gives rise to a relative repulsion  $\propto (\delta_A - \delta_B)^2$ , where  $\delta_i \propto \alpha_i$  is the Hildebrand solubility parameter[36]. This enthalpic incompatibility is inversely proportional to the temperature  $T$ . It may be supplemented by entropic effects: If the monomers have different shapes, like monomers tend to pack more efficiently than unlike monomers. This effect has been studied in detail within a lattice model by Freed and coworkers[28]. Similarly, stiffness disparities tend to favor demixing, as has been shown within P-RISM theory[37]: When mixed with stiff polymers, the more flexible polymers loose conformational entropy, and even though the

stiff polymers win entropy in return, the net effect turns out to be negative. Fredrickson, Liu, and Bates pointed out that phase separation in blends with components of different flexibility or architecture is also promoted by long range composition correlations[38]. The entropic contribution to the incompatibility of polymers has no direct temperature dependence. An indirect temperature dependence may enter through the chain stiffness. The sum of entropic and enthalpic contributions will thus generally lead to a complicated temperature behaviour[28].

The incompatibility of polymers in a binary A/B-blend is often described in terms of a single Flory-Huggins parameter  $\chi$ . It has originally been derived from a simple lattice model on the base of three assumptions[1]:

- (i) The distribution of polymer conformations does not depend on the composition of the blend.
- (ii) Composition correlations are neglected.
- (iii) All monomers have equal size (one lattice site per monomer), and the melt is incompressible (*i.e.*, the lattice is fully occupied by monomers).

The approximation (ii) implies, first, that nonlocal correlations induced by the chain connectivity (the ‘‘correlation hole’’) are ignored, and second, that short range composition correlations related to local demixing tendencies are disregarded (‘‘random mixing’’). One obtains the free energy of mixing per site

$$F_{FH}/(k_B T) = \frac{\phi_A}{N_A} \ln(\phi_A) + \frac{\phi_B}{N_B} \ln(\phi_B) + \chi \phi_A \phi_B, \quad (1)$$

where  $\phi_i$  is the volume fraction and  $N_i$  the chain length of component  $i$ , and the last term describes the loss of enthalpy upon mixing. Assuming that neighbour monomers  $i$  and  $j$  interact with the interaction energy  $\epsilon_{ij}$ , the Flory-Huggins parameter  $\chi$  is given by

$$\chi = \frac{z-2}{k_B T} \left( \epsilon_{AB} - \frac{\epsilon_{AA} + \epsilon_{BB}}{2} \right), \quad (2)$$

with the coordination number  $z$  of the lattice. Equation (2) takes into account that the interaction of a monomer with its two neighbours along the same chain should not contribute to the energy of mixing. The free energy (1) describes usual demixing behaviour, with a miscibility gap at  $\chi$  parameter values larger than

$$\chi_c = \frac{1}{2} \left( \sqrt{\frac{1}{N_A}} + \sqrt{\frac{1}{N_B}} \right)^2. \quad (3)$$

In the one phase region, the  $\chi$  parameter can be determined, *e.g.*, from the small angle structure factor[39]. As long as  $\chi$  is used as an adjustable, heuristic

parameter, this simple model is found to perform extremely well in comparison with experiments. The value of  $\chi$  itself is theoretically less accessible. For example, neutron scattering data reveal in apparent contradiction with Eqn.(2) that  $\chi$  may depend significantly on the composition of the blend[40, 41, 42].

However, this apparent failure is not surprising, since the crudest version of the Flory theory disregards a number of effects which influence real polymeric fluids. In particular, the relative repulsion between polymers of different type depends on the number and the character of contacts between polymers. One can distinguish between different factors.

First, the total volume (at given constant pressure) or the pressure (at given constant volume) of the mixture depends on the composition of the blend. This effect is commonly referred to as the “equation-of-state” effect. Experiments are usually conducted under constant pressure conditions, whereas simulations and analytic calculations often use a simulation box of fixed volume. Since the thermodynamics of mixtures is conceptually simpler at constant pressure  $p$ , we shall mostly discuss the  $NpT$  ensemble in this section. We will relate our conclusions to constant-volume simulations later. At a given pressure, the different components will generally have different monomer densities  $\varrho_A^*$  and  $\varrho_B^*$  in the pure states, and the volume per monomer in the mixture is to lowest approximation the appropriately weighted average of  $1/\varrho_A^*$  and  $1/\varrho_B^*$ . In addition, the incompatibility of unlike chains often leads to an “excess volume on mixing”  $v_{\text{exc}}$ . As we shall see, the composition dependence of  $v_{\text{exc}}$  is roughly parabolic,  $v_{\text{exc}} \approx \tilde{v}\rho(1 - \rho)$ . All taken together, the density  $\varrho$  of the mixture is given by

$$1/\varrho = \rho/\varrho_A^* + (1 - \rho)/\varrho_B^* + \tilde{v}\rho(1 - \rho), \quad (4)$$

where  $\rho$  is the *number* fraction of monomers  $A$ . Since the number of contacts per polymer is proportional to the density, the composition dependence of  $\varrho$  translates directly into a composition dependence of the  $\chi$  parameter in blends of polymers with dissimilar monomer structure,  $\varrho_A^* \neq \varrho_B^*$ . Thus  $\chi$  should depend linearly on the composition of the blend. The linear contribution vanishes in blends of monomers with very similar monomer structure, *e.g.*, isotopic blends or saturated hydrocarbon mixtures, and the remaining composition dependence is parabolic[42]. This is indeed observed experimentally[40, 41]. Equation-of-state effects are thus apparently responsible for the linear part of the composition dependence of  $\chi$ . However, the magnitude of experimentally observed parabolic contributions cannot be explained by Eqn.(4) alone[43].

A second important factor is the local structure of the fluid, *i.e.*, the form of the correlation functions. Let us first note that the demixing is mainly driven by the *intermolecular* contacts between monomers of *different* chains. The *intramolecular* contacts contribute to the conformational free energy of single chains, which does not change very much upon mixing, since conformational changes are generally not very high[44]. In the simplest approximation, the

pair distribution of monomers  $i$  and  $j$  from different chains is assumed to have the form

$$\varrho_{ij}^{(2),inter}(r) = \varrho_i \varrho_j g_{ij}^{inter}(r) \quad \text{with} \quad g_{ij}^{inter}(r) \equiv g^{inter}(r), \quad (5)$$

where the pair correlation function  $g^{inter}(r)$  depends neither on the type  $i$  and  $j$  of the monomers nor on the composition. It is normalised such that  $g(r) \rightarrow 1$  for  $r \rightarrow \infty$ . In real fluids, this approximation will fail in two respects: First, the local *packing* of chains depends on the chain species, either directly due to monomer structure differences (monomer size etc.), or as a more subtle result of chain structure differences (chain architecture, chain stiffness). For example, the position of the peak in the correlation function which corresponds to the first coordination shell depends on the size of the central monomer[45]. The reasons for non-random packing are generally entropic: Excluded volume effects (related to the effective monomer sizes), effects of chain conformational entropy[46] etc. Energetic interactions usually do not affect the packing very much. A particularly strong effect on the demixing behaviour can be expected if like monomers pack closer than unlike monomers. Monte Carlo studies have shown that such “non-additive packing” alone is sufficient to bring about phase separation[46, 47]. Second, even if the local fluid structure is preserved, *i.e.*, the sum  $\sum_j \varrho_{ij}^{(2),inter}(r)/\varrho_i$  is independent of  $i$ , one still expects local composition fluctuations. Such “non-random-mixing” also affects the demixing behaviour[43], especially very close to the critical point[48]. According to the Ginzburg criterion[18], however, the random-mixing approximation becomes better upon increasing the chain length[49].

To summarize, demixing in polymer blends occurs for energetic and entropic reasons. The energetic factors include: Energetic incompatibility of monomers, and shifts of the ratio between inter- and intramolecular monomer contacts, caused by conformational changes. The entropic factors include: Entropic incompatibility of monomers (*e.g.*, due to non-additive packing), packing inhomogeneities due to the different chain structure, and conformational changes of the chain. A huge amount of theoretical work has been devoted to elucidate the effect and the importance of the different contributions[28, 31, 50]. In most cases, the energetic or entropic incompatibility of *monomers* dominates the demixing behaviour. On the other hand, details of the monomer interactions are irrelevant on the scale of whole chains. It is thus reasonable to retain the spirit of the Flory theory and absorb the microscopic details into a few effective parameters, *e.g.*, the  $\chi$  parameter and the compressibility. These can be used as input parameters into theories of more complex systems such as polymer interfaces and surfaces. In addition, they allow to relate simulations of coarse-grained polymer models to experimental systems and idealised theories.

The problem remains to calculate  $\chi$  for a given simulation model. Obviously, Eqn.(2) cannot be used for any model different from the Flory lattice

model. However, the extension of the Flory theory to continuous space models or more sophisticated lattice models is relatively straightforward. This shall be demonstrated in the following. We emphasise that we do not aim to present a complete theory of the  $\chi$  parameter, nor to review the state of the art of generalised Flory theories. Rather, we wish to present a simple “recipe” for the calculation of  $\chi$ , one which takes into account the dominant contributions, and thus gives good results for most practical purposes. In fact, our type of approach has usually provided a good quantitative understanding of simulation data in the past[46, 49, 51, 52, 53].

We consider a mixture of  $n_A$ ,  $n_B$  polymers of length  $N_A$ ,  $N_B$ . Polymers  $k$  are characterised by their center of mass position  $\vec{R}_k$  and the relative coordinates of the monomers  $\vec{u}_{j,k} = \vec{r}_{j,k} - \vec{R}_k$ . The general partition function of such a system in the given volume  $V$  can be written in the form

$$\mathcal{Z} = \frac{(V/V_0)^{n_A+n_B}}{n_A!n_B!} \exp(-m f(\rho, \varrho)), \quad (6)$$

where  $m = n_A N_A + n_B N_B$  is the total number of monomers in the system,  $V_0$  is an arbitrary reference volume, and  $f(\rho, \varrho)$  is defined by

$$e^{-m f(\rho, \varrho)} = \prod_{k=1}^{n_A+n_B} \int_{\Omega} d^3[\frac{\vec{R}_k}{V^{1/3}}] \left\{ \prod_{j=1}^{N_k} \int d^3 \vec{u}_{j,k} \right\} e^{-\beta U[\{\vec{r}_{j,k}\}]} \quad (7)$$

with  $\beta = 1/k_B T$  and the total energy  $U$ . Note that the center of mass positions  $\vec{R}_k$  have been rescaled such that the integration volume  $\Omega$  does not depend on the volume  $V$  any more. The Helmholtz free energy thus reads

$$\beta F = n_A \ln\left(\frac{n_A}{V/V_0}\right) + n_B \ln\left(\frac{n_B}{V/V_0}\right) + m f(\rho, \varrho). \quad (8)$$

The first two terms describe the combinatorial entropy of mixing and the translational entropy of the center of mass of polymers. The last term subsumes the remaining contributions to the free energy, *i.e.*, the internal energy and the conformational entropy. Since both are proportional to the number of monomers  $m$ , it is conveniently expressed in terms of a “monomer free energy”  $f(\rho, \varrho)$ , which depends on the total density  $\varrho$  and the number fraction of  $A$  monomers  $\rho$ . The pressure  $p$  at volume  $V$  is given by

$$\beta p = -\frac{\partial}{\partial V} \beta F = \varrho \left( \frac{\rho}{N_A} + \frac{1-\rho}{N_B} + \varrho \frac{\partial f}{\partial \varrho} \right). \quad (9)$$

and the compressibility  $\kappa$  by

$$\beta \kappa^{-1} = \varrho \frac{\partial \beta p}{\partial \varrho} = 2\beta p + \varrho^3 \frac{\partial^2 f}{\partial \varrho^2}, \quad (10)$$

where terms of order  $1/N$  (ideal gas contributions) have been neglected. Equation (9) can be used as an implicit expression for the density  $\varrho(\rho, p)$ , as a

function of composition  $\rho$  and pressure  $p$ . At constant pressure, the Gibbs free energy per monomer  $\mu$  then reads

$$\beta\mu(\rho, p) = \frac{\rho}{N_A} \ln\left(\frac{\rho\varrho V_0}{N_A}\right) + \frac{1-\rho}{N_B} \ln\left(\frac{(1-\rho)\varrho V_0}{N_B}\right) + f(\rho, \varrho) + \frac{\beta p}{\varrho}. \quad (11)$$

One obtains the excess free energy of mixing

$$\begin{aligned} \beta\mu^{\text{exc}} &\equiv \beta\mu(\rho, p) - \rho\beta\mu(1, p) - (1-\rho)\beta\mu(0, p) & (12) \\ &= \frac{\rho}{N_A} \ln\left(\rho\frac{\varrho}{\varrho_A^*}\right) + \frac{1-\rho}{N_B} \ln\left((1-\rho)\frac{\varrho}{\varrho_B^*}\right) + \beta p v_{\text{exc}} \\ &\quad + [f(\rho, \varrho) - \rho f(1, \varrho_A^*) - (1-\rho) f(0, \varrho_B^*)] & (13) \end{aligned}$$

with the densities of the pure component melt  $\varrho_A^*$  and  $\varrho_B^*$ , and the excess volume on mixing per monomer  $v_{\text{exc}}$ .  $\mu^{\text{exc}}$  can be used to define an effective Flory Huggins parameter  $\chi_{\text{eff}}$

$$\beta\mu^{\text{exc}} = \frac{\rho}{N_A} \ln \phi + \frac{1-\rho}{N_B} \ln(1-\phi) + \chi_{\text{eff}} \rho(1-\rho), \quad (14)$$

where  $\phi$  is the *volume* fraction of monomers  $A$ .

$$\phi = \frac{\rho}{\varrho_A^*} \left/ \left( \frac{\rho}{\varrho_A^*} + \frac{1-\rho}{\varrho_B^*} \right) \right. \quad (15)$$

The temperature dependence and the phase behaviour results from the interplay between the enthalpic and entropic contributions. Since the entropy of mixing is proportional to the inverse chain length, entropic contributions of different origin to the effective Flory-Huggins parameter  $\chi_{\text{eff}}$  are much more important in macromolecular blends than in mixtures of small molecules.

In order to proceed, it will be useful to expand  $f(1, \varrho_A^*)$  and  $f(0, \varrho_B^*)$  around  $\varrho$ . Using Eqns.(9) and (10), and dropping terms of order  $1/N$ , this yields

$$f(\rho, \varrho_i^*) \approx f(\rho, \varrho) + \frac{\beta p}{\varrho_i^*} \left(1 - \frac{\varrho}{\varrho_i^*}\right) + \frac{1}{2\varrho_i^*} (2\beta p - \beta\kappa_i^{-1}) \left(1 - \frac{\varrho}{\varrho_i^*}\right)^2. \quad (16)$$

with the compressibilities of the pure component systems  $\kappa_i$ . Furthermore, we define the difference between volumes per monomer in the pure  $A$  and  $B$  melt,  $\delta = 1/\varrho_A^* - 1/\varrho_B^*$ , and assume that both  $\delta$  and the volume change upon mixing  $v_{\text{exc}} = 1/\varrho - \rho\varrho_A^* - (1-\rho)/\varrho_B^*$  are small. To second order in  $\varrho\delta$  and  $\varrho v_{\text{exc}}$ , one obtains

$$\beta\mu^{\text{exc}} = \frac{\rho}{N_A} \ln \phi + \frac{1-\rho}{N_B} \ln(1-\phi) + \Delta f(\rho, \varrho) + \beta\mu_{\text{comp}}^{\text{exc}} \quad (17)$$

with  $\Delta f(\rho, \varrho) = [f(\rho, \varrho) - \rho f(1, \varrho) - (1-\rho) f(0, \varrho)]$

and the equation-of-state contribution

$$\begin{aligned} \mu_{comp}^{exc} \approx & \frac{1}{2} \varrho \delta^2 \rho(1-\rho) [(1-\rho)\kappa_A^{-1} + \rho\kappa_B^{-1}] \\ & + \frac{1}{2} \varrho v_{exc}^2 [\rho\kappa_A^{-1} + (1-\rho)\kappa_B^{-1}] \\ & + \delta v_{exc} \rho(1-\rho) [\kappa_B^{-1} - \kappa_A^{-1}]. \end{aligned} \quad (18)$$

So far, these are general thermodynamic considerations. The next step is to evaluate  $\Delta f(\rho, \varrho)$  and  $v_{exc}$ . It is at this point that we introduce the generalised Flory Huggins approximation. First, we adopt the Flory assumption (i) and neglect conformational changes upon mixing; hence intrachain interactions do not contribute to the free energy. Second, we assume that species dependent interactions between monomers can be treated as perturbations of a reference system "0" of polymers made of identical monomers[54].

We suppose that we can choose a reference system with a short range monomer potential  $u_0(r)$ , *e.g.*, a hard core potential, which does not distinguish between monomers of different type. We further suppose that the correlation functions  $g_{ij}^{inter,0}(r)$  for interchain contacts and  $g_{ii}^{intra,0}(r)$  for intrachain contacts, and the "bare" incompatibility  $\Delta f^0(\rho, \varrho)$  in the reference system, are known. The correlation functions are related to the monomer pair distribution  $\varrho^{(2)}(r)$  *via*

$$\varrho^{(2)}(r) = \varrho^2 \rho_i \rho_j g_{ij}^{inter,0}(r) + \varrho \rho_i \delta_{ij} g_{ii}^{intra,0}(r), \quad (19)$$

where  $\delta_{ij}$  is the Kronecker symbol. They are independent of the composition  $\rho$  in symmetrical systems, but they may have a (weak) composition dependence if the polymers  $A$  and  $B$  have different architecture or stiffness. In practice,  $\Delta f^0(\rho, \varrho)$  is very small and can usually be neglected, and  $g_{ij}^0(r)$  can be approximated by the correlation functions  $g_{ij}(r)$  measured in simulations of the "full" system [49, 53].

Next, monomer specific "nonbonded interactions" are turned on. One has to distinguish between two possible factors: The monomers may have different size, *i.e.*, the excluded volume interactions may depend on the type of the monomers, and additional energetic interactions may be present which also distinguish between monomers. The excluded volume part of the interaction will be strong, but short ranged, whereas the energetic part may be extended, but weak. It is thus advantageous to separate the total monomer potential  $u_{ij}(r)$  into three parts

$$u_{ij}(r) = u_0(r) + v_{ij}(r) + w_{ij}(r), \quad (20)$$

where  $u_0(r)$  is the potential of the reference system between identical monomers of radius  $d$ ,  $v_{ij}(r)$  is short ranged and nonzero only in a small region  $\xi d$  around  $r = d$ , and  $w_{ij}(r)$  is weak. We will borrow concepts from perturbation expansions in the theory of simple liquids[55] and proceed in two steps: First,

we include the potential  $v_{ij}(r)$  and expand to lowest order in  $\xi$ . Then, we use this system as the new reference system and expand to lowest order in  $w_{ij}$ .

In order to do so, we introduce the indirect correlation function for interchain correlations[55]

$$y_{ij}^{inter,0}(r) = g_{ij}^{inter,0}(r) \exp(\beta u_0(r)), \quad (21)$$

and, analogously, the indirect correlation function for intrachain correlations  $y_{ii}^{intra,0}(r)$ . In simple liquids,  $y_{ij}(r)$  has the advantage of being continuous even in hard core systems. We shall assume that this holds also for polymer melts. In systems of polymers with equal stiffness, in particular, the interchain correlation functions in the polymer melt can be related to the corresponding monomer correlation function  $y_{\text{mono}}(r)$  via [1, 31, 49]

$$y_{ij}^{inter,0}(r) = y_{\text{mono}}(r) \left( 1 - \frac{1}{r} \tilde{g}_{ij} \left( \frac{r}{\sqrt{N}} \right) \right), \quad (22)$$

where  $\tilde{g}_{ij}$  are smooth functions (see also Sec.4). If the monomers have hard core interactions,  $y_{ij}(r)$  outside the core is simply the pair correlation function, and good estimates for the value of  $y_{\text{mono}}$  inside can be looked up in the literature [55]. We now consider a “primed” intermediate system, in which  $v_{ij}(r)$  is turned on, and  $w_{ij}(r)$  is still set to zero. The perturbation expansion to lowest order in  $\xi$  yields the monomer free energy

$$\begin{aligned} f'(\rho, \varrho) &= f^0(\rho, \varrho) + \frac{1}{2} \int dr \{ e^{-\beta u_0(r)} - e^{-\beta(u_0(r)+v_{ij}(r))} \} \\ &\times \left[ \varrho \sum_{i,j} \rho_i \rho_j y_{ij}^{inter,0}(r) + \sum_i \rho_i y_{ii}^{intra,0}(r) \right] \end{aligned} \quad (23)$$

and the indirect correlation function  $y'_{ij}(r) \approx y_{ij}^0(r) + \mathcal{O}(\xi^2)$  (cf [55]). Here the sum runs over  $i, j = A, B$  and  $\rho_i$  is the number fraction of component  $i$ , i.e.,  $\rho_A = \rho$  and  $\rho_B = (1 - \rho)$ . Corrections due to the chain connectivity[56] are of order  $1/\sqrt{N}$  and will be ignored here. The pair correlation function in the primed system thus takes the form  $g'_{ij}(r) = y_{ij}^0(r) \exp[-\beta(u_0(r) + v_{ij}(r))]$ .

We use the primed system as the new reference system and expand  $f(\rho, \varrho)$  in lowest order of  $w_{ij}(r)$

$$f(\rho, \varrho) = f'(\rho, \varrho) + \frac{\beta}{2} \int dr w_{ij}(r) \{ \varrho \sum_{i,j} \rho_i \rho_j g'_{ij}{}^{inter}(r) + \sum_i \rho_i g'_{ii}{}^{intra}(r) \}. \quad (24)$$

After putting everything together, we get to lowest order

$$f(\rho, \varrho) = f^0(\rho, \varrho) + \frac{\varrho}{2} \sum_{i,j} \rho_i \rho_j \gamma_{ij}^{inter}(\rho) + \frac{1}{2} \sum_i \rho_i \gamma_{ii}^{intra}(\rho) \quad (25)$$

with effective interaction parameters  $\gamma_{ij}(\rho)$

$$\gamma_{ij}(\rho) = \int dr y_{ij}^0(r) \{ \exp(-\beta u_0(r)) - \exp(-\beta u_{ij}(r)) \}. \quad (26)$$

The latter may depend weakly on the composition  $\rho$  *via* the pair correlation function  $g_{ij}^0(r)$ . It will prove useful to introduce the quantity

$$\begin{aligned} \mathcal{X} = & 2\gamma_{AB}^{inter}(\rho) - \gamma_{AA}^{inter}(\rho) - \gamma_{BB}^{inter}(\rho) \\ & + [(\gamma_{AA}^{total}(\rho) - \gamma_{AA}^{total}(1))/(1-\rho) + (\gamma_{BB}^{total}(\rho) - \gamma_{BB}^{total}(0))/\rho], \end{aligned} \quad (27)$$

where  $\gamma_{ii}^{total}(\rho)$  is defined as the sum  $\gamma_{ii}^{total}(\rho) = \gamma_{ii}^{inter}(\rho) + \gamma_{ii}^{intra}(\rho)/\varrho$ . Note that the bracketed term vanishes in symmetrical mixtures. In general, it is small and approaches a constant as  $\rho \rightarrow 0$  or  $\rho \rightarrow 1$ .

We are now in the position to calculate the volume change upon mixing  $v_{exc}$  and the volume difference  $\delta$  between the two pure component systems. Eqns.(25) and (10) inserted into Eqn.(9) yield the composition dependence of the density

$$\varrho = \varrho_0 \left( 1 - \frac{\kappa}{2\beta} \left[ \varrho_0^2 \sum_{i,j} \rho_i \rho_j \gamma_{ij}^{inter}(\rho) + \varrho_0 \sum_i \rho_i \gamma_{ii}^{intra}(\rho) \right] \right), \quad (28)$$

where  $\varrho_0$  is the density in the reference system. Using this expression, we obtain

$$\delta = \frac{1}{\varrho_A^*} - \frac{1}{\varrho_B^*} \approx \frac{\varrho\kappa}{2\beta} (\gamma_{BB}^{total}(0) - \gamma_{AA}^{total}(1)) \quad (29)$$

$$v_{exc} = \frac{1}{\varrho} - \frac{\rho}{\varrho_A^*} - \frac{1-\rho}{\varrho_B^*} \approx \frac{\varrho\kappa}{2\beta} \mathcal{X} \rho(1-\rho). \quad (30)$$

In particular, we recover the roughly parabolic composition dependence of  $v_{exc}$  announced above. Note that these equations relate equation-of-state effects at constant pressure to quantities which are accessible in constant-volume simulations. Dudowicz and Freed [28] have studied the volume change of mixing in detail for a lattice model within lattice cluster theory. They find that  $v_{exc}$  is slightly asymmetric, but the approximation by a parabolic law is still reasonable. Unfortunately, they do not calculate the compressibility and the correlation functions, thus we cannot relate Eqn.(30) quantitatively to their work.

These results can be inserted into Eqn.(14). The effective Flory Huggins parameter then takes the form

$$\chi_{eff} = \frac{\varrho}{2} \mathcal{X} + \frac{\Delta f^0(\rho, \varrho)}{\rho(1-\rho)} + \frac{\varrho^3 \kappa}{8\beta} [(\gamma_{AA}^{total}(0) - \gamma_{BB}^{total}(1))^2 + \mathcal{X}^2 \rho(1-\rho)]. \quad (31)$$

The first term comprises the incompatibility of monomers and usually dominates by far. It contains equation-of-state effects in part *via* the prefactor  $\varrho$ . The second term results from packing inhomogeneities due to the different chain structure, and the last term subsumes additional compressibility effects. Effects of conformational changes on mixing are disregarded, and so are non-random-mixing effects, which would be of higher order in the perturbation

expansion. Since the monomer contribution is generally much stronger than the other, the simplified version of Eqn.(31)

$$\chi_{\text{eff}} \approx \frac{\varrho}{2} \mathcal{X} \quad (32)$$

yields a good estimate of the Flory Huggins parameter in most cases.

Most simulations as well as analytical self-consistent field [21, 22, 23] and P-RISM[31] calculations are performed at constant volume. Here, the situation is slightly different: The free energy of mixing is the difference between the Helmholtz free energy of a mixed system at density  $\varrho$ , and between the sum of free energies of the corresponding pure component systems at densities  $\varrho_A^*$  and  $\varrho_B^*$ , where the average density is  $\varrho$ , but the two pure systems are at *pressure* equilibrium with each other. In other words, the pressure of the pure systems  $p^*$  is different from that of the mixed system,  $p$ , and chosen such that there is no volume change on mixing. Thus Eqn.(17) has to be replaced by

$$\begin{aligned} \frac{F_{\text{exc}}}{m} &= \frac{\rho}{N_A} \ln \phi + \frac{1-\rho}{N_B} \ln(1-\phi) \\ &+ [ f(\rho, \varrho) - \rho f(1, \varrho_A^*) - (1-\rho) f(0, \varrho_B^*) ], \end{aligned} \quad (33)$$

where  $\varrho_A^* = \varrho(\rho = 1, p^*)$  and  $\varrho_B^* = \varrho(\rho = 0, p^*)$  are evaluated from Eqn.(9), and the pressure  $p^*$  is determined implicitly through the constraint

$$\frac{\rho}{\varrho_A^*} + \frac{1-\rho}{\varrho_B^*} = \frac{1}{\varrho}. \quad (34)$$

The effective  $\chi$  parameter can then be calculated in the same way as before (in Sec.2.1). One obtains an expression similar to (31), with different compressibility contributions. The situation is particularly simple for mixtures with  $\varrho_A^* = \varrho_B^*$ . Eqn (34) then implies  $\varrho = \varrho_A^* = \varrho_B^*$ , and the effective  $\chi$  parameter is given by

$$\chi_{\text{eff}} = \frac{\varrho}{2} \mathcal{X} + \frac{\Delta f^0(\rho, \varrho)}{\rho(1-\rho)}. \quad (35)$$

We will present some applications of these considerations to simulation models in section 4.1.

### 3 Models and technical aspects

Polymeric materials are characterised by widely spread length and time scales[57, 58, 59]. They range from the size of the chemical subunits (about  $\text{\AA}$ ) to the coil size of the order  $100\text{\AA}$ . In mixtures, the correlation length of composition fluctuations becomes even larger very close to the critical demixing point. Finally, the length scale which characterises the morphology of an immiscible blend is macroscopic, and crucially determines the properties of the material.

The corresponding time scales range from the vibrations of chemical bonds ( $10^{-14}s$ ) to the time needed for macroscopic phase separation, *i.e.*, hours, days or even longer.

A unified theoretical treatment spanning the whole range of length scales is clearly not feasible. Fortunately, polymeric materials share a variety of different dynamic and static properties, which can be traced back to a few relevant polymeric properties. This justifies the description of polymer mixtures on a coarse-grained length scale, using appropriate coarse-grained parameters. One of them is the  $\chi$  parameter, which has been discussed in the previous section, others will be introduced shortly. On that level, the study of coarse-grained polymer models can contribute to a better understanding of the blend properties in two ways:

First, one needs to establish the relation between the chemical structure of polymers and the coarse-grained parameters. Unfortunately, a quantitative prediction of, *e.g.*, the Flory-Huggins parameter  $\chi$ , from the atomistic structure is extremely difficult. This is because the typical energy scale for intermolecular interactions on the monomer scale is of the order  $k_B T$ , whereas the Flory-Huggins parameter is typically 3-5 orders of magnitude smaller in dense polymer blends. Here, coarse-grained models which incorporate some degree of fluid-like structure or conformational asymmetry provide useful qualitative information about the relation between the microscopic structure and the coarse-grained parameters.

Second, the models can be used to study the interplay between the coarse-grained parameters and the bulk thermodynamics and interfacial structure. Such investigations yield valuable insight into the universal material properties in polymeric systems. They can be compared to predictions of mean-field theories or experimental results. This aspect is the focus of most simulations presented here.

A minimal set of relevant polymeric properties comprises: The connectivity of the macromolecules along the backbone, the excluded volume of the segments, and short range thermal interactions. Coarse-grained models, which retain these macromolecular properties, have proven extremely efficient in investigating the universal thermodynamic properties of polymeric multicomponent systems. Only a small number of parameters is required to compare experiments, simulations and theory quantitatively on this coarse-grained level.

These are, for example, the  $\chi$  parameter, the compressibility, and the chain length. In inhomogeneous polymer melts an addition parameter is required which sets the length scale in the system. A natural choice is the extension of single chains, *i.e.*, the end to end distance  $R_e$  of a bulk chain, or equivalently, the gyration radius  $R_g$ . In a dense melt, sufficiently long and flexible chains are well described by random walks[1]. Thus  $R_e$  and  $R_g$  depend on the degree of polymerisation  $N$  like  $R_e = b\sqrt{N}$  and  $R_g = b\sqrt{N/6}$ , where the proportionality constant  $b$  is called the statistical segment length. The two parameters

$\chi N$  and  $R_e$  are generally sufficient to describe inhomogeneous systems of long, flexible polymers with weak monomer interactions (Gaussian chain model). Here, “weak” means that the length scale for composition changes is several times the statistical segment length, *i.e.*,  $\chi \ll 1$ . If the chains are very stiff[99], or the incompatibility is quite large[53], a second length scale may come into play, the persistence length  $\xi$ , which characterises the length of the chain over which the monomers are still strongly correlated[100].

A minimal polymer model, which retains the above properties, is the lattice model of Flory and Huggins[26]. A small number of chemical subunits is represented by a single lattice site on a simple cubic lattice. The excluded volume property is mimicked by the constraint of single site occupancy, and bonded segments occupy nearest neighbour sites on the lattice. Phase separation is caused by unfavourable interactions between neighbour segments of different type. In spite of its extreme simplicity, this model and its mean-field analysis by Flory and Huggins is usually the basis for discussions of polymer miscibility in melts, and it already yields many important informations on the bulk thermodynamics (see section 2.). In particular, the Flory Huggins theory predicts a linear increase of the critical temperature of a binary polymer blend with the degree of polymerisation, in agreement with experiments[60] and simulations[48].

Lattice models which resemble the Flory-Huggins-model have been used in simulations of polymer melts and solutions. One prominent example is the Larson model, which has found wide application for the study of amphiphilic systems (for a recent review see[34]).

However, many important properties of polymer melts cannot be represented in such a simple model[61]: The small number of bond angles does not allow for a realistic modelling of the bending rigidity or other structural asymmetries. Monomers and vacancies have the same size, hence the underlying monomer fluid displays no packing effects[62]. These are however crucial ingredients to the Flory-Huggins parameter, as discussed above. With the constraint that the bond length is always one lattice unit, the implementation of a local diffusive monomer dynamics is not possible. The latter is needed when studying the collective dynamics of phase separation (*i.e.*, spinodal decomposition), or the relation between the thermodynamic state and the single chain dynamics.

The bond fluctuation model (BFM) of Carmesin and Kremer[63] overcomes the above mentioned limitations while retaining the computational advantages of a lattice model: Each monomer blocks eight corners of a whole unit cell in a simple cubic lattice from further occupancy. Monomers along a polymer are connected by one of 108 bond vectors of length 2,  $\sqrt{5}$ ,  $\sqrt{6}$ , 3, or 10. Due to the size difference between vacancies and monomers, one gets fluid-like packing effects. The extended monomer size and the variety of possible bonds helps washing out the underlying lattice structure. A local monomer hopping dynamics can be implemented, which leads to a Rouse-like dynamics in dilute

solutions.

At the volume fraction 0.5 or monomer number density  $\rho = 0.5/8$  (the factor 8 reflects the monomer volume), the model mimics many properties of a concentrated polymer solution or melt. The excluded volume interaction is screened down to about 6 lattice spacings, *i.e.*, the chains have Gaussian statistics on larger length scales. The diffusion of very long chains exhibits the signature of reptation-like motion: the entanglement length is roughly 32 monomers[64]. Due to the relatively high number of remaining vacancies, the polymer conformations still equilibrate reasonably fast. Real polymer systems can be mapped onto the BFM[65, 66]. One monomer then corresponds to 3-5 chemical repeat units, and one lattice units to roughly 2 Å. In the following, all lengths shall be given in units of the lattice constant.

The BFM has been widely used to study the statics and dynamics of polymer solutions[67, 64], melts[64, 68], and glasses[69]. Hence, a variety of properties of the model are known, and this established model is well suited to test theories of polymer miscibility and polymer interfaces.

Due to the high number of possible bond vectors, one has 87 different bond angles. This allows for a rather realistic modelling of a local stiffness along the chain. Unless noted otherwise, all of the polymers are complete flexible. In some of our studies[46, 53], we impose on the  $B$  component of the blend an intramolecular potential, which favours straight bond angles:  $E(\Theta) = f \cos(\Theta)$ , where  $\Theta$  denotes the complementary angle between successive bonds. On increasing the strength of this potential from  $f = 0$  (flexible) to  $f = 2$ , the chain extension increases by a factor 1.5 (for chain length  $N = 32$ ).

We shall consider binary polymer mixtures containing  $n_A$   $A$ -polymers of length  $N_A$  and  $n_B$   $B$ -polymers of length  $N_B$ , and ternary systems with additionally  $n_C$  symmetric  $AB$  diblock copolymers of length  $N_C$ . In some applications, the stiffness of the  $B$  component is tuned through the bond angle potential described above. The two kinds of monomer species,  $A$  and  $B$ , interact *via* a square well potential. The range of the potential corresponds roughly to the first coordination shell of the monomer fluid, and includes the 54 nearest lattice sites. Unless noted otherwise, monomers of the same type attract each other, whereas contacts between unlike species increase the energy

$$-\epsilon_{AA} = -\epsilon_{BB} = \epsilon_{AB} \equiv \epsilon. \quad (36)$$

In the following, we measure all energies in units of  $k_B T$ . Hence,  $\epsilon$  is proportional to the inverse temperature.

One might argue that purely attractive monomer interactions of different strength would mimic the experimental situation in a more realistic way. The choice (36) is motivated by the following consideration: Even the pure one component system ( $\rho = 0$  or  $\rho = 1$ ) is in fact a mixture of homopolymers and vacancies. For strong attractive interactions between monomers, one hence encounters a liquid-vapour phase separation into a homopolymer-rich and

vacancy-rich phase. The temperature of this “ $\Theta$  transition” is independent of the chain length ( $\epsilon_{\Theta} \approx 0.495(5)$ [67]), whereas the temperature of the AB unmixing transition increases like  $N$ . For long chains, these two temperature scales are thus well separated. For short chains, however, the choice of purely attractive monomer interactions would lead to a rather complicated interplay between both transitions. It is thus expedient to choose the interactions such that the demixing occurs already at rather weak absolute values of  $\epsilon_{ij}$ . Simulations of the Bond fluctuation model have also been performed using a slightly smaller interaction range. The results for strictly symmetric interactions are qualitatively similar[48, 49].

Even though complex lattice models capture many of the relevant properties of polymer mixtures, there are limitations: Constant pressure simulations of lattice models[70] are difficult, whereas their implementation is relatively straightforward for off-lattice models. Keeping the pressure constant is desirable, for example, when the blend exhibits a pronounced volume change upon mixing (cf. section 2.). Even at constant volume, off-lattice models have the advantage that the pressure and the interfacial tension can be measured *via* the virial equation[47, 71]. Furthermore, they lend themselves to molecular dynamics simulations, which are able to capture hydrodynamic flow. The latter is crucial, for example, to describe the final stage of spinodal decomposition[72]. On the other hand, off-lattice simulations are more demanding with respect to computational resources. In many respects, the BFM simulations are remarkably consistent with off-lattice predictions, *e.g.*, with respect to the packing contributions to the  $\chi$  parameter (see Sec.4.1).

In studies of the thermodynamics and structure of polymer blends, two statistical ensembles are mainly used: In the canonical ensemble, the temperature, the volume and the global composition of the mixture are fixed, and the Monte Carlo moves update the polymer conformations. In simulations of the BFM, local monomer hops[63] and slithering snake-like movements[73] have been applied. The former allow an interpretation of the Monte Carlo simulation in terms of an overdamped, purely diffusive dynamics, the latter relax the polymer conformations faster by a factor  $N$ . In off-lattice models, MD integration[47] is often employed to propagate the system. The canonical ensemble is useful for the study of dynamic properties, the local interfacial structure and the phase behaviour of systems with strong structural asymmetries[53].

In systems with weak or moderate structural asymmetry, however, the phase behaviour is investigated more efficiently in the semi-grandcanonical ensemble[74]: The temperature, the volume, and the total number of monomers are held constant, while the composition of the mixture is allowed to fluctuate. In binary mixtures, it is controlled by just one parameter, the exchange monomer potential  $\Delta\mu$  (see Eqn. (49)). In ternary mixtures, a second variable  $\delta\mu$  has to be introduced, which couples to the copolymer content in the mixture. The Monte Carlo scheme includes moves which turn polymers of type

$A$  into polymers of type  $B$  and vice versa, and additional moves in ternary systems which switch between homopolymers and copolymers[75]. This algorithm has first been introduced by Sariban and Binder[74], and applied to the simple Flory-Huggins lattice model of strictly symmetric binary blends. In that case, the semi-grandcanonical identity switches are merely a change of the polymer label. It literally carries over to off-lattice models of symmetric mixtures[47]. The scheme can also be applied to asymmetric mixtures with different dispersion forces[76], with chain length asymmetry[49, 73], with stiffness disparity[46], and non-additive monomer shapes[46]. For even stronger asymmetries, configurational bias[67] or gradual inserting schemes can be envisaged. For very strong conformational asymmetries, however, the semi-grandcanonical moves become increasingly inefficient[53].

The advantages of the semi-grandcanonical ensemble are threefold[46, 75]:

First, since the global composition is not conserved, large length scale composition fluctuations relax much faster than in the canonical ensemble. The attempt to observe an unmixing transition driven just by the diffusion of polymers poses a substantial challenge in terms of computational resources[61]. Furthermore, a thorough analysis of finite-size effects in the canonical ensemble (*e.g.*, via a subbox analysis[77]) requires formidably large system sizes. The semi-grandcanonical ensemble concentrates the computational effort on the composition fluctuations, the slowest mode in the blend. Sophisticated finite-size scaling methods have been applied to study the crossover from mean-field to Ising critical behaviour in strictly symmetric polymer mixtures[48], and mixed-field finite-size techniques have been used to accurately determine the critical point in asymmetric mixtures[67, 78, 79]. These techniques can be combined with a multi-histogram extrapolation of the joint energy-composition distribution[61, 80] and hence allow to determine the phase behaviour accurately from simulations of systems of rather modest size (*i.e.*, comprising only a few hundred polymers).

Second, the semi-grandcanonical equation of state, which relates the composition  $\rho$  to the chemical potential difference  $\Delta\mu$ , can be measured in semi-grandcanonical simulations. This gives information about the thermodynamics of mixing, and provides the most direct connection to mean-field theories. In particular, it can be used to relate simulations to the considerations of Sec. 2 (see also Sec. 4.1).

Third, the semi-grandcanonical ensemble can be combined with multi-canonical reweighting schemes[81]. Rather than generating configurations following the Boltzmann distribution, the simulation then samples the phase space according to the probability  $\exp(-(E - n_A\Delta\mu)/k_B T)/W(\rho)$ , where  $E$  denotes the total energy of the binary system. By choosing the preweighting factors  $W$  proportional to the equilibrium probability distribution in the semi-grandcanonical ensemble  $P(\rho)$ , one achieves uniform sampling of all compositions  $\rho$ . An excellent estimate for the equilibrium probability distribution can be obtained from histogram extrapolations of previous runs. Below the

critical temperature, this Monte Carlo scheme[51, 75] encourages the system to explore configurations in which the two phases coexist in the simulation box.

We shall illustrate the last point with the simulation data for a symmetric ternary homopolymer/copolymer blend. The probability distribution of the composition as a function of the chemical potential  $\delta\mu$  of the copolymers is presented in Fig.1 on a logarithmic scale. We have chosen an elongated simulation cell[75] of  $xy$ -cross section  $L^2$  and extension in  $z$ -direction  $2L = 96$ . The distributions exhibit two pronounced peaks corresponding to the composition of the two coexisting phases. In the two-domain state between these coexistence compositions, the probability is strongly reduced. For large enough system sizes, the probability distribution there is dominated by configurations containing two interfaces parallel to the  $xy$  plane, as sketched schematically in the figure (periodic boundary conditions are applied). The two interfaces of area  $L^2$  separate the two bulk coexisting phases. The probability of these configurations with respect to the bulk is reduced by the Boltzmann weight  $\exp(-2L^2\sigma/k_B T)$  of the interfacial free energy cost[82], where  $\sigma$  is the interfacial tension between the coexisting phases. Hence, the interfacial tension can be calculated from

$$\frac{\sigma}{k_B T} = \frac{1}{2L^2} \ln \left( \frac{P(\rho_{\text{coex}})}{P(1/2)} \right). \quad (37)$$

The plateau in the probability distribution around  $\rho = 1/2$  shows, that the two interfaces can vary their mutual distance, thereby changing the composition, without free energy costs. This important consistency check indicates that the the interfaces can be described as flat and non-interacting. The free energy of the interface is lowered upon increasing the copolymer chemical potential. Within the same simulation run, we can determine how the number of copolymers at fixed chemical potential  $\delta\mu$  depends on the composition. (cf. Fig. 1 (b)). Not surprisingly, configurations with two interfaces contain more copolymers. From this we can extract the excess of copolymers at the interface. It grows upon increasing the chemical potential  $\delta\mu$  of the copolymers. Similarly, we can monitor the energy as a function of the composition, and extract the excess energy of the interface. In addition, a careful analysis of the probability distribution yields information about the interaction potential (joining pressure) between two interfaces. Hence, bulk and excess interfacial properties are simultaneously accessible in the semi-grandcanonical ensemble[75].

The same combination of techniques has been applied to thin film, where both flat walls attract the same component[83]. In this case the coexistence chemical potential  $\Delta\mu_{\text{coex}}$  is shifted from its bulk value  $\Delta\mu_{\text{coex}}^b = 0$ , but nevertheless reweighting techniques permit to locate the phase coexistence accurately even for low temperatures.

Even with a careful choice of the statistical ensemble and the use of recently

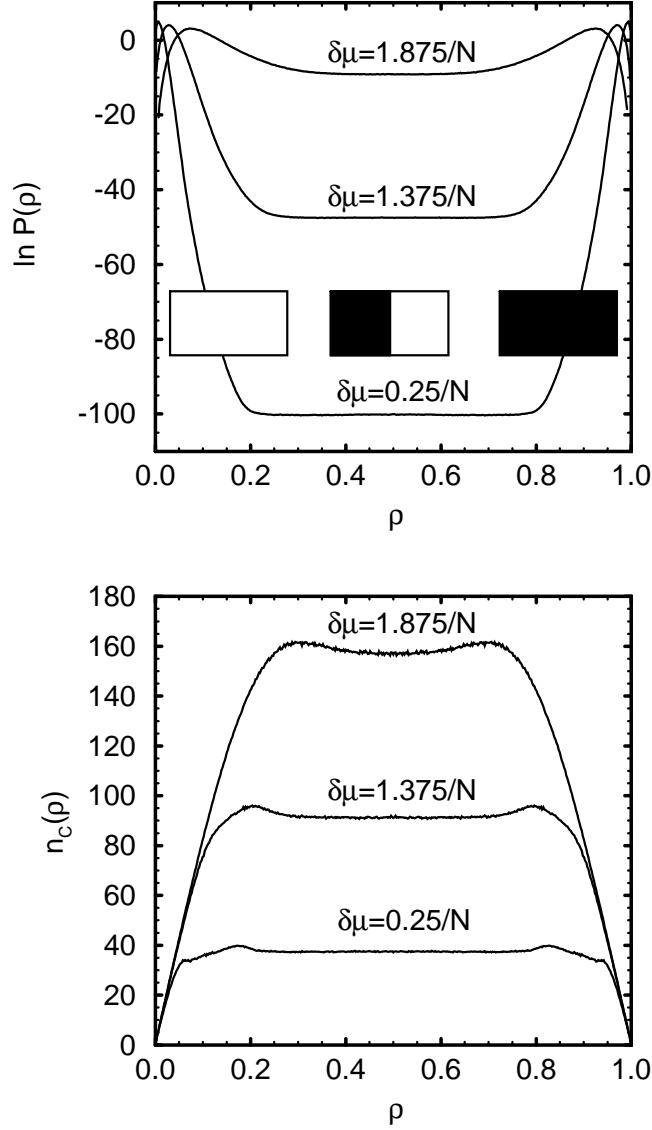


Figure 1: (a): Probability distribution of the composition in a ternary homopolymer-copolymer mixture at  $\epsilon = 0.054$  and system size  $48 \times 48 \times 96$ . Upon increasing the chemical potential  $\delta\mu$  of the copolymer, the “valley” in the probability distribution becomes shallower, indicating that the copolymers decrease the interfacial tension. (b): Average number of copolymers  $n_C(\rho)$  as a function of the composition for the same system as in (a).  
From Ref. [75].

developed simulation and analysis techniques, the accurate measurement of structural and thermodynamical properties in the computer simulation poses huge computational demands. On the one hand, very large system sizes are required to investigate, *e.g.*, the effect of capillary-wave broadening. In our simulations[51, 86, 117] we vary the lateral extension of the simulation box from 64 to 512 lattice units. The largest simulation cell contains more than a million monomers. Only massively parallel computers like the CRAY T3D/T3E make the simulations of such large systems feasible. Using a two-dimensional geometric parallelisation scheme, we have efficiently implemented the local monomer movements. Even for small simulation cells, the program scales practically linear with the number of processors up to 256[84]. On the other hand, many systems are characterised by protracted long time scales: Increasing the chain length  $N$  increases dramatically the relaxation times of the chain conformations. Deutsch et al. have employed chains of up to 512 segments to investigate the crossover between mean-field and Ising critical behaviour. Their investigation required several thousand hours of CRAY Y-MP time[48]. The equilibration of long wave length interfacial fluctuations is also difficult because of its slow dynamics. Another example is the relaxation time in the framework of the multicanonical reweighting scheme[81]. In the most ideal case, the system performs a random walk on all compositions. Therefore the correlation time scales with the system size  $L$  like  $L^6$ . The total amount of CPU time investigated into the results presented in the following exceeds the equivalent of  $10^5$  hours on a single CRAY T3D processor.

In blends with strong structural asymmetries (*e.g.*, large stiffness disparity, polymer solvent systems), the semi-grandcanonical identity switches between different polymer types are rather inefficient[46, 53]. Hence, methods for measuring the interfacial tension in the canonical ensemble have been explored. In off-lattice models, the interfacial tension can be measured via the anisotropy of the pressure tensor. This method has been successfully applied to determine the free energy costs of a hard wall[71] in a concentrated polymer solution and the interfacial tension[47] in a binary polymer blend. However, the generalisation to lattice models is difficult[70].

An alternative way of measuring the interfacial tension is the analysis of the capillary fluctuation spectrum[53, 75, 85]: In general, interfaces are not flat, but exhibit long-wavelength capillary-wave fluctuations. A typical snapshot of the local interfacial position in a binary polymer blend is presented in Fig.2. The local interfacial position has been laterally averaged over a size comparable to the polymer's radius of gyration, and large length scale fluctuations are clearly visible[86]. Let us consider a flat interface, neglect bubbles and overhangs, and describe the local deviations of the interfacial position from its lateral average by the single valued function  $u(x, y)$ . Due to the local deviations, the interfacial area is increased compared to the corresponding planar interface. The effect on the thermodynamics of the interface is commonly described by the capillary-wave Hamiltonian for long-wavelength

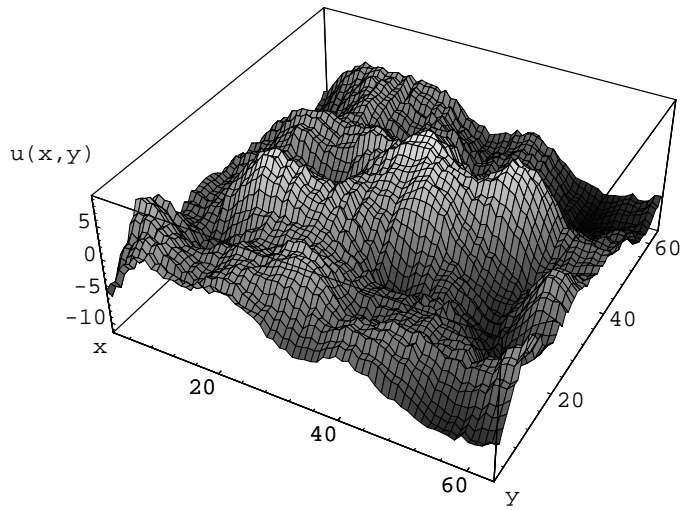


Figure 2: Typical snapshot of the local interfacial position  $u(x, y)$  for a system of lateral extension  $L = 64$ ,  $\epsilon = 0.03$  and  $N = 32$ . The coarse-graining size  $B = 8$  corresponds roughly to the chain's radius of gyration. Long wavelength fluctuations are clearly visible. From Ref. [117].

interfacial fluctuations[87, 88]

$$\mathcal{H} = \int dx dy \left\{ \frac{\sigma}{2} (\nabla u)^2 \right\}, \quad (38)$$

where  $\sigma$  denotes the effective interfacial tension. It can be diagonalised very naturally with a simple Fourier transform

$$u(x) \sim \frac{a_0}{2} + \sum_{l=0}^{L/2-1} \{a(q_l) \cos(q_l x) + b(q_l) \sin(q_l x)\}, \quad (39)$$

with  $q_l = 2\pi l/L$ . The equipartition theorem shows that the Fourier components have a Gaussian distribution with Gaussian width

$$\frac{2}{L^2 \langle a(q)^2 \rangle} = \frac{2}{L^2 \langle b(q)^2 \rangle} = \frac{\sigma}{k_B T} q^2. \quad (40)$$

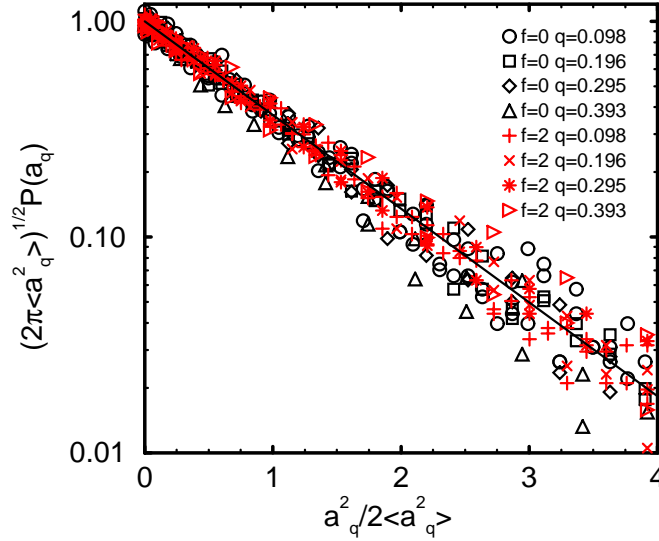


Figure 3: Probability distribution of Fourier components  $a(q)$  and  $b(q)$  of the local interfacial position for the four smallest wave-vectors  $q$  in a system with system of lateral size  $L = 64$ , bending energies  $f = 0, 2$ , and chain length  $N = 32$ . For the data collapse the  $1/q^2$  dependence of the variance has been exploited. The solid line shows the expected Gaussian distribution.

From Ref. [53].

The probability distribution for the Fourier components of the local interfacial position are presented in Fig.3 for a symmetric blend and a blend with

strong stiffness disparity[53]. In both cases, the long-wavelength interfacial fluctuations are well described by the quadratic interfacial Hamiltonian. The interfacial tension can be determined from the inverse width of the distribution. For the symmetric blend, this value can be compared with the independent measurement in the semi-grandcanonical ensemble. The agreement is very good. The interfacial fluctuation spectrum thus provides an efficient alternative way of measuring the interfacial tension in structurally asymmetric systems. For example, the method has been successfully applied to measure the interfacial tension of amphiphilic bilayers[85].

We note that the relative increase of the interfacial area is proportional to  $\ln L/L^2$ . Hence interfacial excess quantities[75] (*e.g.*, the interfacial tension, the excess energy of the interface, the enrichment of copolymers or vacancies) are rather insensitive to capillary fluctuations. Interfacial profiles are affected more dramatically[86]. “Apparent” profiles obtained *via* lateral averaging depend sensitively on the extension of the system and are significantly broader than the “intrinsic” profiles. This capillary-wave broadening has to be accounted for when comparing simulation results analytical predictions, and is also relevant for the interpretation of experiments. The fluctuations of the local interfacial position  $\langle u^2(x, y) \rangle$  are obtained by integrating over the lateral Fourier components. The power law spectrum in Eqn.(40) leads to logarithmic divergencies for  $q \rightarrow 0$  and  $q \rightarrow \infty$ . We can remove these divergencies by introducing heuristic cut-offs  $q_{\max}$  and  $q_{\min}$ , and obtain

$$\langle u^2(x, y) \rangle = \frac{k_B T}{2\pi\sigma} \ln \left( \frac{q_{\max}}{q_{\min}} \right). \quad (41)$$

The lower cut-off  $q_{\min}$  is simply determined by the system size, *i.e.*,  $q_{\min} = \frac{2\pi}{L}$ . The value of the upper cutoff  $q_{\max}$ , however, is less obvious. In addition to long-wavelength capillary fluctuations, one has composition fluctuations on short length scales at the interface (*i.e.*, intrinsic fluctuations), which determine the shape of the intrinsic interfacial profile. The upper cutoff  $q_{\max}$  is hence related to the lateral length scale which separates the intrinsic fluctuations from the fluctuations of the center of the intrinsic profile. For small molecules and far from the critical region, one usually estimates  $q_{\max} = 2\pi/a$ , where  $a$  denotes the molecular extension. In polymeric systems[86], however, three possible microscopic length scales have to be considered: the statistical segment length  $b$ , the width of the intrinsic interfacial profile  $w_0$ , which is controlled by the Flory-Huggins parameter, and the radius of gyration, which scales like  $\sqrt{N}$ . Semenov[89] proposed to use  $q_{\max} = 2/w_0$  as the upper cutoff. In principle, Monte Carlo simulations could address this problem by studying the dependence of the broadening on the chain length  $N$  and the incompatibility  $\chi$ .

A finite bending rigidity  $\kappa$  of the interface also generates a smooth cutoff of the fluctuation spectrum on small length scales. This effect can be described

by the Helfrich Hamiltonian[88]

$$\mathcal{H} = \int dx dy \left\{ \frac{\sigma}{2} (\nabla u)^2 + \frac{\kappa}{2} (\Delta u)^2 \right\}. \quad (42)$$

Including the bending rigidity  $\kappa$  removes the divergency for  $q \rightarrow \infty$ . A similar analysis as above yields

$$\frac{2}{L^2 \langle a(q)^2 \rangle} = \frac{\sigma}{k_B T} q^2 + \frac{\kappa}{k_B T} q^4 \quad \text{and} \quad \langle u^2(x, y) \rangle = \frac{k_B T}{2\pi\sigma} \ln \left( \frac{\sqrt{q_{\min}^2 + \sigma/\kappa}}{q_{\min}} \right). \quad (43)$$

Thus the crossover length  $\sqrt{\sigma/\kappa}$  acts as upper cutoff  $q_{\max}$ . This effect is important in interfaces with absorbed amphiphilic molecules[75]. At high concentrations, they oppose themselves to being squeezed together on one side of a bent interface, thus generating a positive contribution to the bending rigidity (cf. Sec. 4.3).

The laterally averaged ‘‘apparent’’ profile can be approximated by the convolution of the intrinsic profile  $\rho_0(z)$  with the Gaussian distribution  $P(u)$  of the local interfacial position

$$\rho(z) = \int du \rho_0(z - u) P(u). \quad (44)$$

For the slope at the center of the profile, this convolution approximation yields in the case of weak broadening[90]

$$\left. \frac{d\rho}{dz} \right|_{z=0} \approx \left. \frac{d\rho_0}{dz} \right|_{z=0} + \frac{k_B T}{4\pi\sigma} \left. \frac{d^3 \rho_0}{dz^3} \right|_{z=0} \ln \left( \frac{q_{\max}}{q_{\min}} \right). \quad (45)$$

The slope at the center ( $z = 0$ ) of the profile can be used to define the inverse interfacial width  $\left. \frac{d\rho}{dz} \right|_{z=0} = \frac{1}{2w}$ . Hence we obtain for the broadening of the apparent profile[86]

$$w^2 \approx w_0^2 + \frac{k_B T}{\pi\sigma} \left| \left. \frac{d^3 \rho_0}{dz^3} \right|_{z=0} \right| w_0^3 \ln \left( \frac{q_{\max}}{q_{\min}} \right) = w_0^2 + \frac{k_B T}{4\sigma} \ln \left( \frac{q_{\max}}{q_{\min}} \right). \quad (46)$$

where we have approximated the shape of the intrinsic profile by an error function in the last step in order to calculate the numerical prefactor.

Since analytic mean-field theories generally yield intrinsic profiles, one has to take due account of the capillary-wave broadening when comparing them with simulation data. In order to reduce the broadening effect, we can define ‘‘reduced’’ profiles by laterally dividing the system into subsystems of size  $B \times B$ [53, 86]. In each subsystem, we localise the interfacial position and average profiles with respect to the local midpoint of the profile. In principle, the lateral length scale  $B$  can be chosen as to match the width of the reduced profile with the theoretically predicted value. However, once  $B$  is chosen in this way, other profiles (*e.g.*, segmental orientations, chain ends, etc.) can be compared to theoretical predictions without any adjustable parameter.

## 4 Simulation results

Many of the simulation and analysis techniques presented in the previous sections can be applied to lattice models of polymers as well as to off-lattice models, and also to non-polymeric models. In this section, we will show how they have been applied specifically to simulations of the bond fluctuation model, and compare the results to experiments and to analytical predictions.

### 4.1 Local packing and miscibility

We will begin with a discussion of the bulk thermodynamics of polymer mixtures. The knowledge of the phase behaviour is required for a discussion of interfacial properties[51], and of considerable interest in itself[48].

In the past, special emphasis has been given to simulations of symmetric, binary polymer blends[48]. Experimentally, nearly symmetric blends can be realised by mixing partially deuterated and protonated polymers[60], or as blends of statistical copolymers[91]. Simulations by Deutsch and Binder[48] have confirmed the linear scaling[26] of the critical temperature by investigating polymers with up to 512 monomers. Using a sophisticated crossover finite-size scaling technique, they accurately located the critical temperature and investigated the crossover between mean-field behaviour to 3D Ising critical behaviour, which prevails in the vicinity of the critical point. Upon increasing the chain length, the Ising critical region shrinks, in accord with the Ginzburg criterion[18] and with experimental observations[60, 92].

The phase behaviour of the bulk is determined by the local structure of the polymeric fluid, as reflected by the fact that the Flory-Huggins parameter  $\chi$  can be related to the intermolecular pair correlation function[49] (see Sec. 2.). In the simplest case of an athermal melt (*i.e.*,  $\epsilon = 0$ ) the intermolecular packing is driven by two effects: On the one hand, the size disparity between vacancies and monomers gives rise to fluid-like packing effects which result in a highly structured correlation function at short distances. On the other hand, the extended structure of the macromolecules causes a reduction of contacts with other chains on intermediate length scales. In order to separate the monomeric, local packing effects from the universal behaviour of the polymeric correlation hole, we consider the ratio between the intermolecular pair correlation function and its monomeric equivalent. As shown in Fig. (4), it is found to be largely independent from the packing of the monomers. Since the correlation hole comprises  $N - 1$  monomers and the only length scale of a flexible Gaussian polymer is its radius of gyration  $R_g \sim \sqrt{N}$ , the reduced correlation function exhibits the following scaling behaviour

$$\frac{g_N(r)}{g_{N=1}(r)} = 1 - \frac{1}{r} \tilde{g} \left( \frac{r}{\sqrt{N}} \right). \quad (47)$$

Fig.4 demonstrates for various chain lengths[49], that such a scaling works very well for flexible chains. We note that the situation is somewhat more

complicated in systems of semiflexible chains, since the correlation hole is characterised by two length scales, the persistence length and the radius of gyration[53].

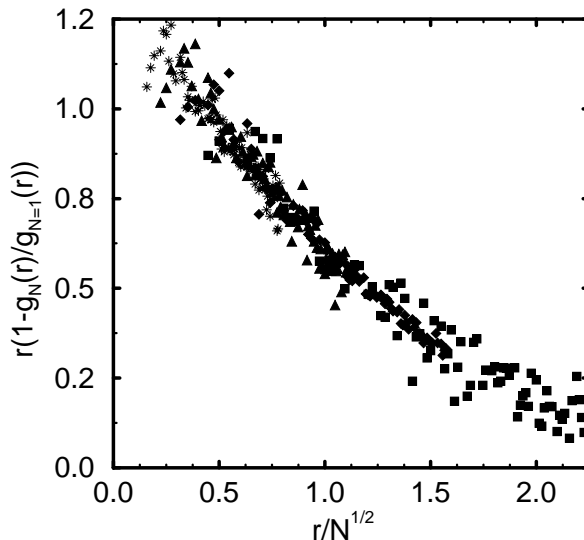


Figure 4: Scaling of the reduced correlation function  $g_N(r)/g_{N=1}(r)$  with chain length.  $N = 20$  (squares),  $N = 40$  (diamonds),  $N = 80$  (triangles), and  $N = 160$  (stars) for athermal ( $\epsilon = 0$ ) melts. From Ref. [49].

The deepening of the correlation hole with increasing chain length induces a chain length dependence of the effective number of intermolecular contacts

$$z = z^\infty + \frac{\text{const}}{\sqrt{N}} \quad (48)$$

and hence presents a correction of relative order  $1/\sqrt{N}$  to the scaling of the critical temperature for flexible chains (see below).

In the following we will present examples for different contributions to the effective  $\chi$ -parameter. In particular, we will consider the “semi-grandcanonical equation of state”, which relates the composition of the blend  $\rho$  to the exchange chemical potential  $\Delta\mu$ ,

$$\beta\Delta\mu = \frac{\partial F_{\text{exc}}/m}{\partial \rho} = \frac{1}{N_A} \ln \phi - \frac{1}{N_B} \ln(1 - \phi) - \chi_{\text{eff}}(2\phi - 1) + C, \quad (49)$$

where  $C$  is a constant. Since this thermodynamic relation is directly accessible in the simulations of the semi-grandcanonical ensemble, we can extract an

effective  $\chi$  parameter. This value can be then compared to Eqn.(35), which relates the local fluid structure to the incompatibility  $\chi$ .

Our first example is a blend of polymers of different chain length ( $N_A \neq N_B$ ), which demix for energetic reasons, *i.e.*, unlike monomers repel each other according to Eqn.(36). Here the athermal ( $\epsilon = 0$ ) system of non-interacting monomers suggests itself as the reference system. The bare contribution  $\Delta f^0$  to the  $\chi$  parameter is negligible, and the pair correlation functions in the reference system do not depend on the identity of the monomers. The combination of Eqns.(26), (27), and (35) then yields the effective Flory Huggins parameter

$$\chi_{\text{eff}} = 2z_c\epsilon, \quad \text{where} \quad z_c = \varrho \int_0^{\sqrt{6}} dr g(r) \quad (50)$$

defines an “effective coordination number”  $z_c$  in the spirit of the original Flory-Huggins theory. We recall the  $g(r)$  is the intermolecular pair correlation function. Fig.5 demonstrates that the equation of state obtained with this value of  $\chi_{\text{eff}}$  is in excellent agreement with the simulation data [49], for temperatures well above the unmixing transition.

The second example illustrates demixing driven by entropic repulsion between monomers. One particularly simple realisation is non-additive packing. In real polymer mixtures, it might arise from disparities in the monomer shape or steric hindrances[28, 93]. It is also used by Grest and coworkers to induce phase separation in an off-lattice model[47]. In our case, it is modelled as follows: Monomers of different type are subject to the additional constraint that they must not come closer than  $\sqrt{5}$  lattice constants, whereas monomers of the same type can approach each other up to 2 lattice constants, as before. The natural reference system is again the athermal system of non-overlapping monomers. Eqns (26), (27) and (35) lead to the entropic  $\chi$  parameter

$$\chi_{\text{eff}} = z_6 \quad \text{with} \quad z_6 = \varrho \int_0^{\sqrt{5}} dr g(r). \quad (51)$$

This non-additive packing thus gives rise to a rather large, positive contribution to the effective Flory-Huggins parameter, and the system demixes. In addition, energetic interactions can be introduced as before. The total effective  $\chi$  parameter is then given by

$$\chi_{\text{eff}} = z_6 + 2\epsilon z_c. \quad (52)$$

The case of *attractive* interaction between unlike monomers (*i.e.*,  $\epsilon < 0$ ) is particularly interesting. Here one encounters a Lower Critical Solution Point (LCSP) upon heating the system, *i.e.*, reducing the strength of the thermal interaction  $\epsilon$ .

Using the intermolecular pair correlation function of a reference system ( $|\epsilon| = 0.05$ , additive), we obtain  $z_6 = 0.238(2)$  and  $z_c = 1.41(2)$  at the

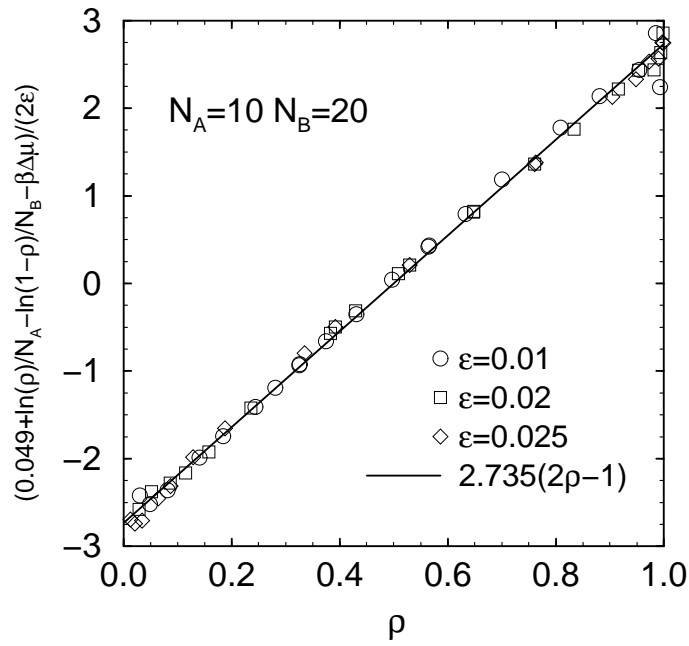


Figure 5: Equation of state for an asymmetric polymer mixture  $N_A = 10$  and  $N_B = 20$  for various temperatures above the critical point.  $\epsilon = 0.01$  (circles),  $\epsilon = 0.02$  (squares),  $\epsilon = 0.025$  (diamonds).  $\epsilon_c = 0.0320(1)$ . The straight line corresponds to the prediction with  $z_c = 2.735$ . From Ref. [49]

monomer volume fraction  $8\varrho = 0.35$ , which corresponds to a concentrated solution. Fig.6 compares the effective  $\chi$  parameter extracted from the semi-grandcanonical equation of state in the one phase region (*i.e.*, at low temperatures) with the above estimate. Eqn.(52) describes the simulation data quite successfully [46]. We note that Eqn. (52) predicts that the critical temperature of the LCSP does not increase upon increasing the chain length, but converges to  $1/T_c = |\epsilon_c| = z_6/2z_c$ . This is indeed found in the simulations, and in qualitative agreement with experiments of Schwahn and co-workers[94] on the phase behaviour of PVME/PS blends.

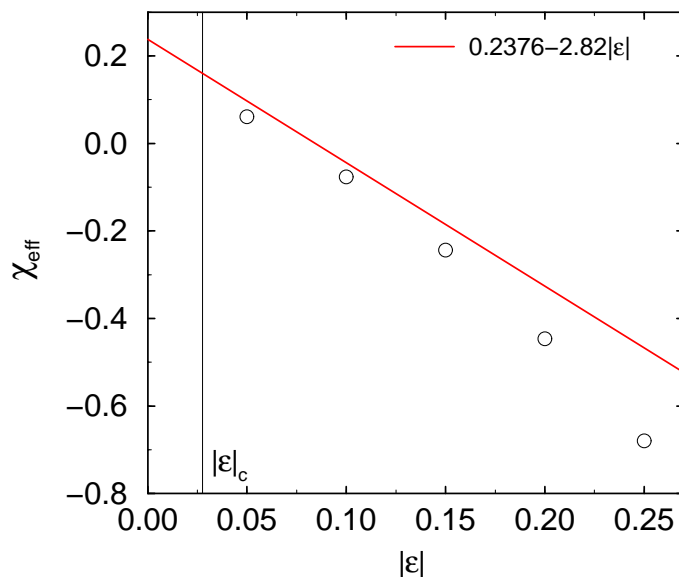


Figure 6: Effective Flory-Huggins parameter extracted from the semi-grandcanonical equation of state for a non-additive polymer mixture of chain length  $N = 20$  at a total monomer density of  $8\varrho = 0.35$ . There is an attraction between unlike monomers ( $\epsilon < 0$ ). Upon heating *i.e.*, reducing the thermal interactions, the blend phase separates. The location of the Lower Critical Solution point is indicated as a vertical line. From Ref. [46].

The last example presents a situation where polymer incompatibility is caused on the level of whole chains as a result of different chain stiffness. Monomers are taken to be identical otherwise. Hence we are left with the “bare” contribution to the  $\chi$  parameter,  $\chi = \Delta f^0(\rho, \varrho)/[\rho(1 - \rho)]$ , which results from packing inhomogeneities due to the different chain structure. The explicit evaluation of this term requires more elaborate techniques[37, 38] than introduced in Sec.2. Fig.7 shows the semi-grandcanonical equation of state

for an athermal (*i.e.*,  $\epsilon = 0$ ) mixture of flexible ( $f = 0$ ) and semiflexible ( $f = 1$ ) polymers. A composition dependence in the figure indicates a non-zero Flory-Huggins parameter. The simulation data clearly show, that the purely entropic packing differences give rise to a small, chain-length independent, positive Flory-Huggins parameter  $\chi$ . Though the effect is quite small, it might lead to phase separation for very long chain lengths  $N > \mathcal{O}(1000)$ . Of course, one could suspect, that these subtle packing effects are strongly influence by the structure of the underlying lattice. However, field theoretical calculations by Liu and Fredrickson[38] as well as recent P-RISM calculations by Singh and Schweizer[37] predict effects of similar magnitude within off-lattice models. Off-lattice simulations by Weinhold et al. [45] also confirm the order of magnitude of the packing induced incompatibility.

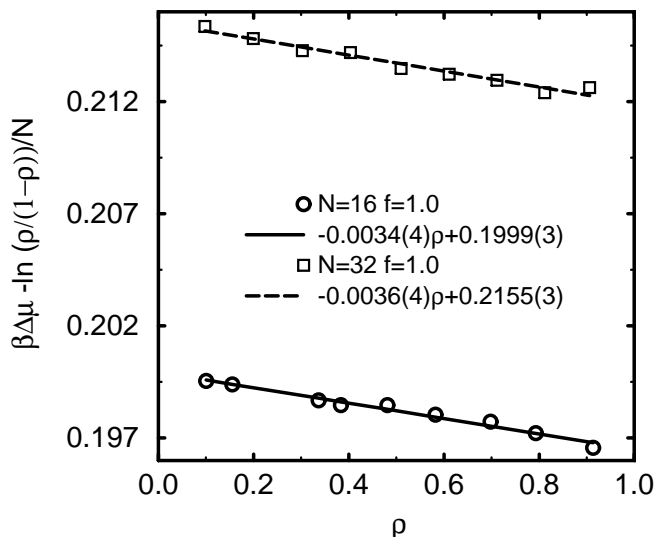


Figure 7: Semi-grandcanonical equation of state for a polymer mixture of flexible ( $f = 0$ ) and semi-flexible ( $f = 1$ ) polymers without thermal interactions ( $\epsilon = 0$ ). The translational entropy is already accounted for and the composition dependence indicates the stiffness-induced contribution to the Flory-Huggins parameter. From Ref. [46].

Since purely athermal systems of flexible and stiff chains with chain lengths accessible to simulations usually don't demix, additional, repulsive monomer interactions have to be turned on in order to induce demixing. The "athermal" system of flexible and stiff chains then has to be used as the reference system[53] (cf. Eqn.(26)). We note that the reference system is asymmet-

ric, and the effective coordination numbers depend on the identity of the monomers and the composition of the blend. This is because stiffer chains are more extended, and folding back is less probable. Hence the number of intermolecular contacts increases and, as a result, the interaction parameter  $\gamma_{ii}$  in (26) is larger for the stiffer species, even if the interaction potentials are chosen symmetric. The effect on the  $\chi$  parameter is comparable in magnitude to the stiffness induced (athermal) contribution discussed above[46] for temperatures of the order  $T_c$ . For strongly incompatible blends, the enthalpic contribution to  $\chi$  dominates.

Fig.8 shows an interface between two demixed phases in a blend of flexible  $A$  and stiff  $B$  chains, confined between hard walls. The two phases are at pressure equilibrium, and vacancies are enriched in the stiffer phase. A similar effect has been observed in an athermal two-dimensional system[95]. It is due to the fact, that the stiffer chains pack less efficiently and hence their osmotic pressure is slightly higher. The order of magnitude of the effect is however only 1 %. The oscillations of the density directly at the walls are packing effects and reflect directly the monomer correlation functions.

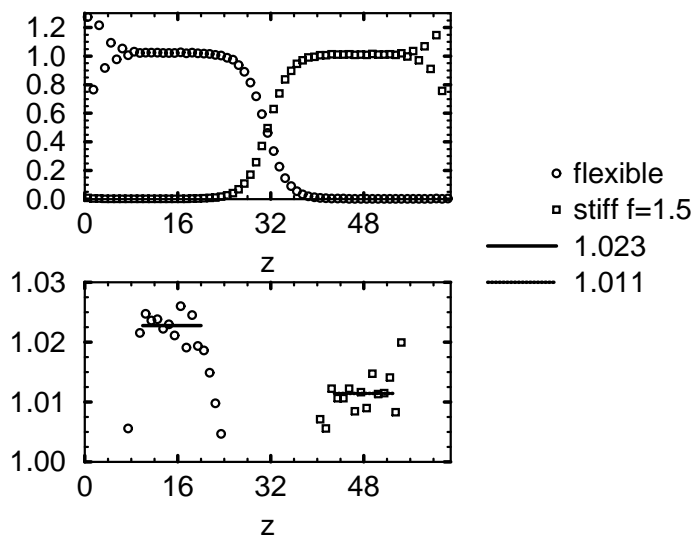


Figure 8: Polymer blend of flexible ( $f = 0$ ) and semi-flexible ( $f = 1.5$ ) polymers ( $N = 16$ ) between two hard and neutral walls well below the critical temperature  $T = 0.346T_c$ . The normalised monomer density profile shows pronounced packing effects at the wall. The blow-up shows that vacancies are enriched in the stiffer phase (right hand side). From Ref. [46].

Simulation studies of polymer compatibility in continuous space and at constant pressure have been performed recently by Kumar[96]. He studies miscible and immiscible blends of Lennard-Jones chains, and finds volume changes of mixing with the expected parabolic composition dependence. He also measures incremental chemical potentials of both components and relates them to an expression similar in spirit to Eqn.(32). Inserting correlation functions which include both interchain and intrachain contacts gives worse results than using correlation functions for interchain contacts only, in agreement with the considerations of Sec. 2. In particular, he studies the special case of a blend with interactions chosen such that  $\mathcal{X}$  happens to cancel to zero[97]. As expected, the volume change of mixing practically disappears. Nevertheless, the blend demixes, if the chains are sufficiently long. The effect can be attributed in part to compressibility effects (*i.e.*, the remaining third term in Eqn. (31)), but probably also involves higher-order effects, such as non-random-mixing and chain-stretching effects. A systematic investigation of the scaling of the critical temperature with chain length would help to separate the different contributions, but has not yet been attempted.

In the above examples we have related the structure of the polymeric fluid to its thermodynamical properties far from the unmixing transition, and obtained a reasonable quantitative agreement. Within mean-field theory, the unmixing temperature is given by Eqn.3.

However, even in the simplest possible systems – strictly symmetric, binary polymer blends – mean-field theory overestimates the critical temperature at short chain lengths[49]. This discrepancy between the mean-field theory and the Monte Carlo results can be attributed to composition fluctuations. The fact that we observe 3D Ising critical behaviour at the unmixing transition already indicates that the deviations from the random-mixing approximation involved in the mean-field theory are quite strong. The effect is well known in mixtures of small molecules, *i.e.*, the small chain length limit of polymer blends. P-RISM calculations[50] and calculations of fluctuation corrections to mean-field by Holyst and Vilgis[98] suggest that these non-random-mixing effects die out with  $1/\sqrt{N}$ . Thus, the ratio between the actual critical temperature and the mean-field value should converge to 1 with a  $1/\sqrt{N}$  correction. This is illustrated in Fig.9 for strictly symmetric models with different interaction range, and for blends with chain length asymmetry[49]. The relative deviation between the critical temperature and its mean-field estimate is the larger, the smaller the interaction range. When the mean-field theory is used to fit Monte Carlo data on the critical isotherm, non-random mixing effects thus lead to a strong parabolic composition dependence of the effective  $\chi$  parameter close to the critical point[48, 49].

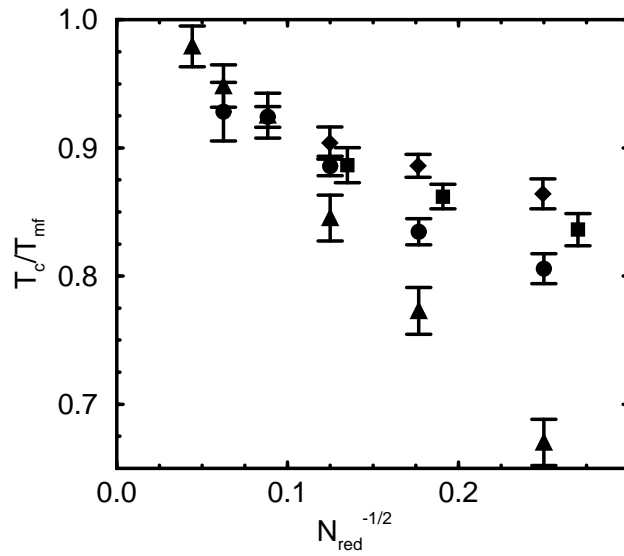


Figure 9: Chain length dependence of the ratio between the critical temperature of a binary polymer blend and the mean-field estimate, which takes the local fluid structure into account. Symmetric mixtures ( $N_A = N_B$ ) are presented by circles and triangles (for a reduced range of the thermal interactions). Asymmetric mixtures with  $N_B = kN_A$  are shown as squares ( $k = 2$ ) and diamonds ( $k = 3$ ).  $N_{\text{red}} = 4N_A N_B / (N_A^{1/2} + N_B^{1/2})^2$ . From Ref. [49].

## 4.2 Homopolymer interfaces

We shall now discuss some general concepts on the structure of interfaces between demixed homopolymer phases. For the sake of simplicity, we will consider a symmetrical system of polymers  $A$  and  $B$  with equal chain length  $N$  and statistical segment length  $b$ . Generalised expressions for asymmetric systems will be given later if necessary. Within the Gaussian chain model, the behaviour of the interface is basically driven by the relative polymer incompatibility  $\chi N$ . One distinguishes the two limiting cases  $\chi N \rightarrow \infty$  (strong segregation limit) and  $\chi N \rightarrow (\chi N)_c$  (weak segregation limit). The two quantities in which we will be interested are the interfacial width and the interfacial tension.

The intrinsic interfacial width  $w$  results from an interplay between entropic factors and “energetic” factors related to the monomer incompatibility, *i.e.*, the  $\chi$  parameter. The interfacial tension,  $\sigma$ , is closely related. It turns out to be roughly proportional to  $m^2/w$ , where  $m = \rho_A^{coex} - \rho_B^{coex}$  is the width of the miscibility gap. In the limit of very long chains, the conformations of chains are strongly perturbed in the vicinity of the interface. Polymers can win conformational entropy by allowing chain portions to loop into the unfavourable side. The entropy gain due to the formation of such loops has to be balanced with the energy loss due to the unfavourable contacts of the loops. Since the total chain length does not enter this argument, the interfacial width is independent of chain length, and so is the interfacial tension. The strong segregation theory ( $2/N \ll \chi \ll 1$ ) yields [21]

$$w_{SSL} = b/\sqrt{6\chi}, \quad \beta\sigma_{SSL} = \sqrt{\chi/6} \varrho b. \quad (53)$$

In the limit of short chains or weak incompatibility, the conformations of chains are only weakly perturbed. Here, polymers as a whole may move over to the unfavourable side, thereby gaining translational entropy. The latter has again to be balanced with the energy loss, and the resulting interfacial width and interfacial tension depend on the distance of  $\chi N$  from the critical point  $(\chi N)_c$ . In the weak segregation limit, one thus gets

$$w_{WSL} \propto (1 - \chi_c/\chi)^{-\nu}, \quad \sigma_{WSL} \propto (1 - \chi_c/\chi)^\mu, \quad (54)$$

with the critical exponents  $\nu = 1/2$ ,  $\mu = 3/2$  and the critical point  $\chi_c = 2/N$  in the mean-field regime. Experiments are usually well described by mean-field exponents, except in the ultimate vicinity of the critical point. In simulations, the chains in the blend are often too short to prevent critical fluctuations, and one finds Ising exponents. In the intermediate region between the weak segregation limit and the strong segregation limit, the contribution of loops competes with an increasing influence of chain ends. Interpolation schemes between the two limits have been suggested by Tang and Freed[101] and more recently by Ermoshkin and Semenov[102]. Numerically, the problem can be treated, *e.g.*, within the self-consistent field theory[21, 22, 23].

From this discussion, it is clear that the properties of interfaces are strongly influenced by their microscopic structure. This interplay has attracted abiding theoretical[21, 22, 23, 24, 25, 101] and experimental[103, 104, 119, 105, 106, 107, 108, 109] interest. Apart from the factors already mentioned, packing and compressibility effects are again important, as well as chain orientations and chain-end distributions. These are all accessible to computer simulations. Unfortunately, simulation studies of polymer interfaces are computationally extremely demanding. Only recently have such simulations been carried out by different groups. The first is due to Reiter and coworkers and treats poly-disperse chains on a lattice model using a bond breaking algorithm[110]. More recently, Ypma et al have performed simulations of a polymer interface confined between a hard wall and a free surface[70]. Grest and coworkers study a polymer interface in a continuous model, in which demixing is driven by non-additive packing[111]. Similar to our simulations[86, 75], they also put particular emphasis on the analysis of the capillary-wave broadening. In general, the results from these simulations agree with our own results obtained with the bond-fluctuation model, which shall be discussed in some detail in the following sections. Simulations of copolymers embedded in a homopolymer interface are even more scarce. In many studies, the homopolymer interface has been approximated by an external potential[112, 113]. Simulations of a copolymer/homopolymer mixture have been performed by Pan et al[114], however, the homopolymer concentration in their study is less than 10 %.

We begin with the discussion of the interfacial properties of a homopolymer interface in a strictly symmetric binary blend. For a structurally symmetric polymer blend, the interfacial tension is accessible *via* the reweighting technique. At the critical point, it vanishes with a critical power law of the form  $\sigma = \hat{\sigma}(\epsilon - \epsilon_c)^\mu$ , where the critical exponent  $\mu = 2\nu = 1.258$  is given by the 3D Ising universality class, and the critical amplitude takes the value  $\hat{\sigma} = 2.9$  for  $N = 32$ . In the strong segregation limit, the self-consistent field theory for Gaussian chains predicts in the long chain limit

$$\sigma_{\text{SSL}} = \varrho \sqrt{\chi/6} \left( \frac{2b_A^2 + b_A b_B + b_B^2}{b_A + b_B} \right), \quad (55)$$

where  $b_A$  and  $b_B$  denote the statistical segment length of the components. For finite chain length  $N$ , however, the interfacial tension is reduced by a factor  $1 - \alpha_\sigma \frac{2}{\chi N}$ . There exist various analytical predictions for the constant  $\alpha_\sigma$ :  $\alpha_\sigma = \ln 2$ [115],  $\alpha_\sigma = \pi^2/12$ [116],  $\alpha_\sigma = 1.35$ [101], and  $\alpha_\sigma = 2 \ln 2$ [102]. In Fig.10 we present the ratio between the measured interfacial tension and the strong segregation estimate, and compare it to the self-consistent field theory[52]. The deviations from the strong segregation result are indeed well described by a correction of the proposed form, and the simulation data as well as the SCF results agree best with a constant  $2 \ln 2$ .

The influence of architectural asymmetry is illustrated in Fig.11. Upon increasing the persistence length of the  $B$  component, the interfacial ten-

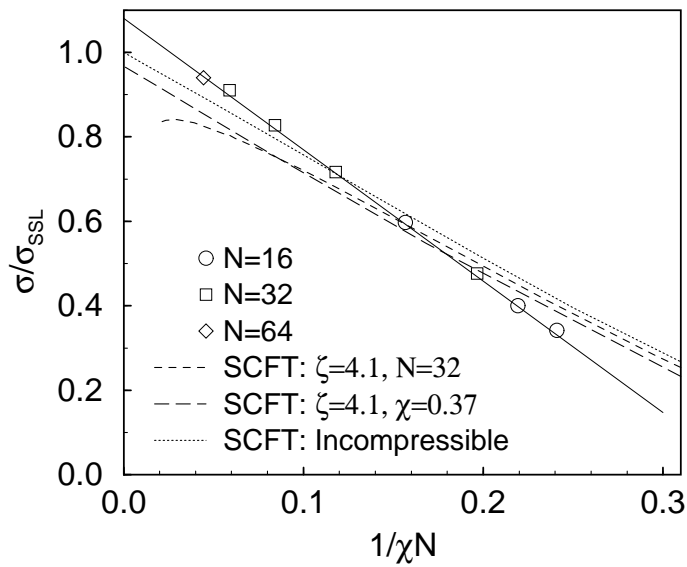


Figure 10: Temperature dependence of the interfacial tension for chain lengths  $N = 16, 32, 64$ . The ratio of the interfacial tension (measured using the reweighting scheme) and the analytical prediction is presented to investigate chain end corrections. The lines correspond to self-consistent field calculations for compressible and incompressible systems. From Ref. [52].

sion increases[53]. The arrow marks the result for symmetrical mixtures obtained *via* the reweighting technique. Note that packing effects, which are induced by the stiffness disparity, increase the incompatibility by a factor of  $\Delta\chi/\chi \approx 7 \cdot 10^{-3}$  for  $f = 1$ [46]. Hence, they are not strong enough to explain the increase of the interfacial tension for this combination of chain length, enthalpic repulsion and stiffness disparity. The simulation data in the figure are compared to numerical self-consistent field calculations (SCF), which take due account of the chain conformations on all lengths scales, and to the analytical prediction for infinitely long Gaussian chains of different statistical segment lengths (cf. Eqn. 55). The self-consistent field theory describes the dependence on the chain architecture almost quantitatively, whereas the analytical calculation captures the qualitative trend, but fails to predict the correct absolute values.

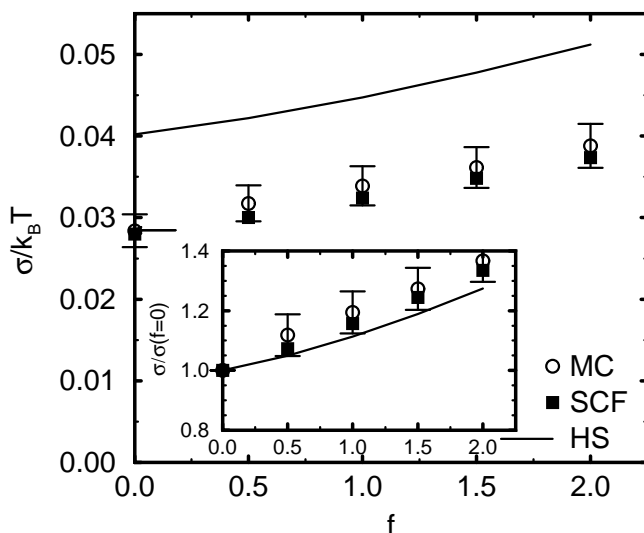


Figure 11: Stiffness dependence of the interfacial tension for chain length  $N = 32$  for rather high incompatibility  $\epsilon = 0.05$ . Circles denote estimates via an analysis of the spectrum of interfacial fluctuations. The arrow marks the independently measured value (em via the reweighting scheme) for the symmetric blend. The data are compared to self-consistent field calculations which take due account of the chain architecture. Also shown is the strong segregation prediction of the Gaussian chain model for blends with different statistical segment length by Helfand and Sapse (HS). The inset presents the relative effect of increasing the stiffness  $f$  of the  $B$  component. From Ref. [53].

These thermodynamic properties do not shed light on the microscopic structure of the interface[117]. However, factors like the width of the interfacial region, the orientations of polymers on different length scales and the enrichment of vacancies or solvent influence the materials properties. Experiments indicate[118], that entanglements in the interfacial zone are of major importance for the mechanical properties of the composite. The distribution of chain ends are important for the interdiffusion and healing properties at interfaces between long polymers. They also play an important role for reactions at interfaces. Chain ends are enriched in the center of interfaces, and this effects goes along with a depletion at a distance  $R_g$  away from the midpoint of the profile. The shape of a polymer is a prolate ellipsoid, which is oriented in the presence of an interface. This is quantified by the orientational parameter

$$q_X(z) \equiv \frac{3\langle X_z^2 \rangle_z - \langle \vec{X}^2 \rangle_z}{2\langle \vec{X}^2 \rangle_z}, \quad (56)$$

where the outer index  $z$  at the brackets denotes the  $z$  coordinate of the vector's midpoint, and the inner indices the Cartesian components of the vector  $\vec{X}$ . The apparent orientation profiles for the end-to-end vector  $\vec{R}_e$  and the bond vectors  $\vec{b}$  are presented in Fig. 12. Both the bond vectors and the end-to-end vector align parallel to the interface. Most notably, the orientation effects are the stronger the larger the length scale[51]. The Gaussian chain model does not predict any orientation of bond vectors, and the observed effect is rather small. The inset shows the predictions[52] of a worm-like chain model for the bond orientation. A rather small bending stiffness is sufficient to describe the simulation data (for chains with bending potential  $f = 0$ ). On the end-to-end vector, however, the interface has a similar effect than a free surface or a hard wall, and induces pronounced alignment.

In blends with stiffness disparity[53] the persistence length of the semi-flexible component introduces a second microscopic length scale into the interfacial profile, which is independent from the interfacial width. In the weak segregation limit, the interfacial width is larger than the persistence length of the semi-flexible component and the interfacial behaviour can be described appropriately within the Gaussian chain model, when the stiffness dependence of the statistical segment length  $b(f)$  is accounted for. Upon increasing the stiffness disparity at fixed incompatibility, the interfacial width increases too. In the strong segregation limit, the interfacial widths becomes narrower than the persistence length and the local chain architecture becomes important. In this highly incompatible regime, the interfacial width decreases upon increasing the stiffness disparity at fixed  $\chi N$ , in qualitative contrast to the predictions of the Gaussian chain model. Self-consistent field calculations which take due account of the chain architecture on all length scales describe the simulation data almost quantitatively[53]. Figure 13 shows bond orientational profiles in a temperature region, where the stiffness disparity hardly affects the width of

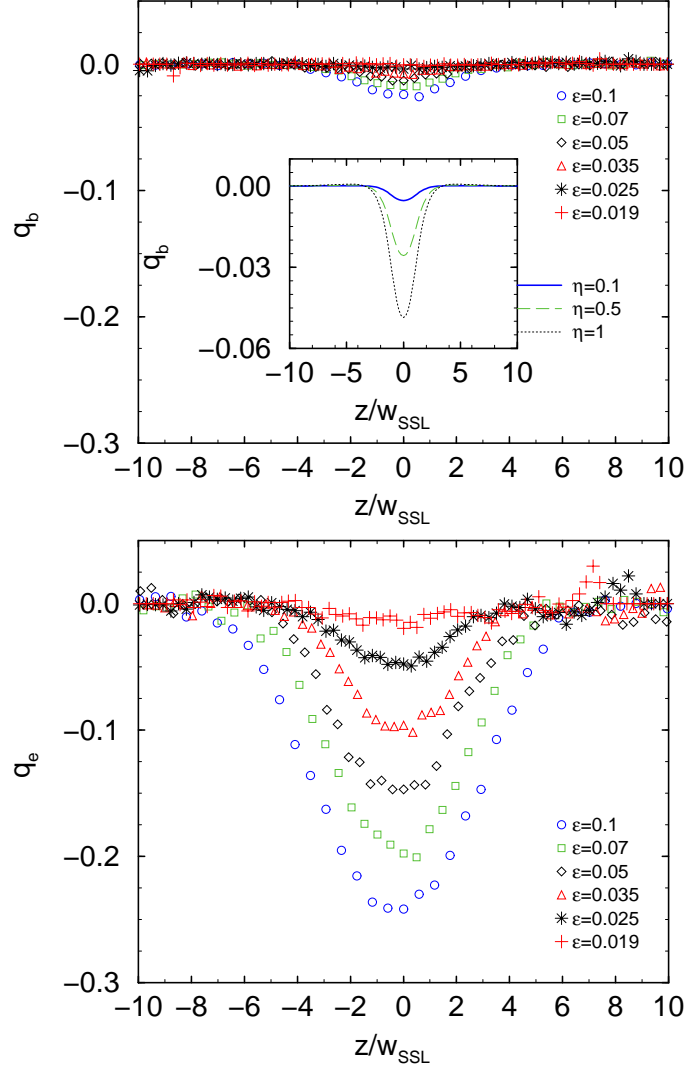


Figure 12: (a): Orientation of bond vectors as a function of the distance from the interface. Apparent profiles for chain length  $N = 32$  are shown for various inverse temperatures  $\epsilon$ . The temperature ranges from the weak segregation limit to the strong segregation limit. The inset presents self-consistent field calculations in the framework of the worm-like chain model for different values of the bending rigidity  $\eta = 0.1, 0.5$  and  $1$ . and  $\epsilon = 0.1$ . (b): Apparent profile for the orientation of the chain's end-to-end vector as a function of the distance from the interface. Polymers align parallel to the interface. Note that the effect is much more pronounced than for the bond vectors.

the composition profile. Upon increasing the bending energy  $f$  of the semiflexible component, the orientation of the semiflexible  $B$  polymers increases, whereas the flexible component remains unaffected. The width of the orientational profiles increases upon increasing  $f$ . The numerical self-consistent field calculations and the reduced interfacial profiles agree almost quantitatively.

Moreover, we find enrichment of vacancies at the interface of our compressible blend. This segregation of vacancies can be qualitatively estimated as follows: By reducing the monomer density  $\delta\rho$ , the system lowers the number of unfavourable contacts between unlike monomer species. This reduces the excess energy density by  $\epsilon w z_c \delta\rho/2$ . The decrease of contact energy contrasts the entropy loss due to the creation of a density fluctuation. The latter can be estimated as  $w\delta\rho^2/2\rho\kappa_T$ , where  $\kappa_T$  denotes the isothermal compressibility. Balancing both contributions[51], we estimate the reduction of the total monomer density  $\delta\rho$  to be of the order  $\chi\kappa_T\rho/2$ . This simple argument is compatible with the simulation data for the total monomer concentration profile, and with self-consistent field calculations for compressible polymer blends.

Finally in this section we discuss the profile of the number of intermolecular contacts across the interface (Fig. 14 [51]). In the weak segregation limit, the number of contacts  $z_c$  is independent of the distance from the interface, whereas it is strongly reduced in the center of the interface at high segregation. This effect does not simply reflect the density reduction at the center of the interface, but is even more pronounced. It results from orientation and conformational changes of the macromolecules at the interface[51]: Polymers rearrange as to exchange energetically unfavourable intermolecular contacts with intramolecular contacts. The latter number is increased at the interface.

### 4.3 Copolymers at interfaces

We will now discuss the effect of adding copolymers to the interface. Such amphiphilic molecules are, of course, most likely to be found at the interface between  $A$  and  $B$  homopolymer regions, where the different blocks can extend into the appropriate volume. This reduces not only their own enthalpy, but also that of the homopolymers which it displaces from the interface. The reduction of the interfacial tension has a strong influence on the morphology of the blend, whereas the entanglement of the individual blocks with the corresponding homopolymers increase the mechanical stability of the composite. The tendency to adsorb at the interface is balanced by the loss of entropy of mixing and of conformational entropy as the copolymers stretch to accommodate a greater areal density. Thus the adsorption at the interface competes with the creation of micelles in the bulk phases. Mean field theories predict that the addition of copolymers drives the system to compatibility in the weak segregation limit, while one encounters a first order transition to a lamellar phase at strong segregation. In the intermediate regime, a complex

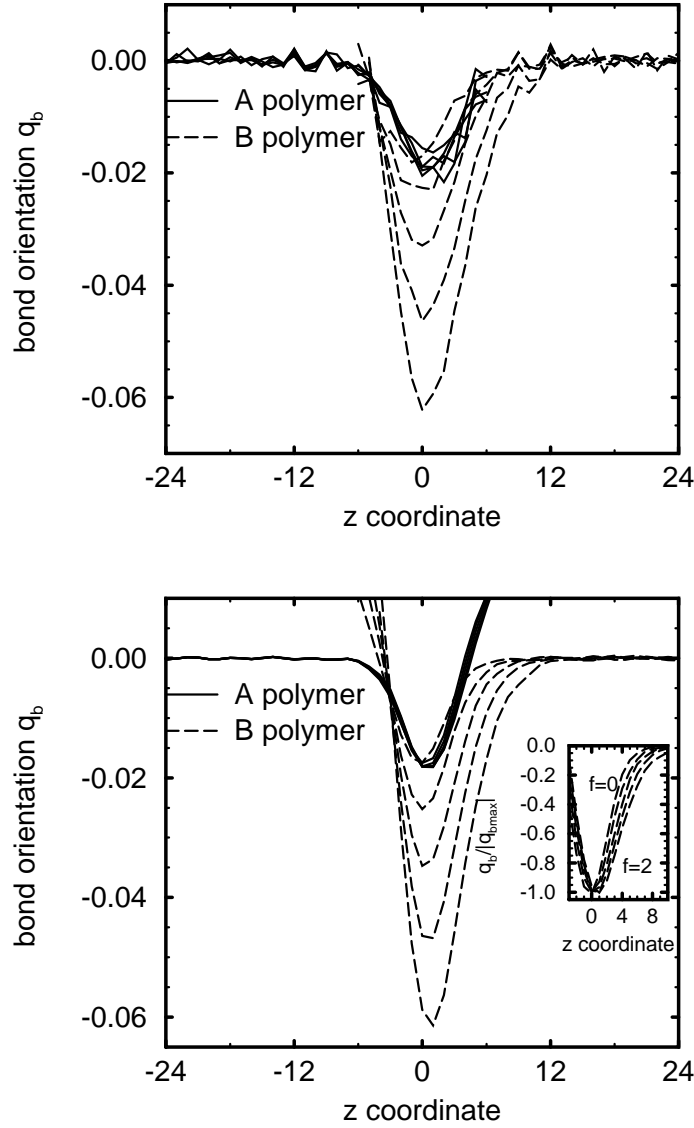


Figure 13: Orientation of bond vectors  $q_b$ , for flexible  $A$ -polymers (solid lines) and semi-flexible  $B$ -polymers (dashed lines) with bending energies  $f = 0, 0.5, 1, 1.5$  and  $2$ . The orientation of the  $B$ -bonds and the length scale of ordering increases upon increasing  $f$ . (a) Monte Carlo results, (b) self-consistent field calculations. The inset shows the self-consistent field results normalised to the maximum of  $q_b$ . Note, that the width of the orientation profile grows upon increasing  $f$ . From Ref. [53].

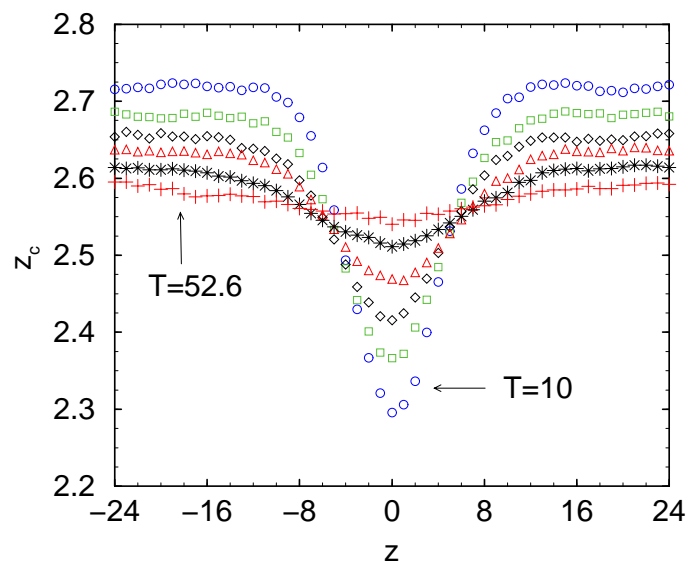


Figure 14: Apparent profiles of the intermolecular contacts for inverse temperatures  $\epsilon = 0.1, 0.07, 0.05, 0.035, 0.025, 0.019$  and chain length  $N = 32$ . Note the pronounced reduction of intermolecular contacts at the center of the interface in the strong segregation limit. From Ref. [51].

phase behaviour is predicted by the theory.

First, we discuss the adsorption of a small amount of copolymers at a strongly segregated homopolymer interface. The areal density  $\nu$  of copolymers is so small, that they do not overlap  $\pi\nu b^2 N/12 \approx 0.3$ . The apparent profiles of the individual segments are presented in Fig.15. Chain ends of the homopolymers  $\rho_e$  are enriched at the interface, whereas the density of middle segments is reduced compared to the total homopolymer density. The copolymers, however, exhibit the opposite trend. The middle segment, which joins the distinct blocks, is enriched at the center of the interface, whereas the chain ends stretch out into their corresponding bulk phases. The inset presents the results of the self-consistent field calculations, which qualitatively agree with the simulation data, except for the fact that they do not capture the capillary-wave broadening. The qualitative behaviour is also born out in experimental findings of Russell[119] and co-workers.

It is instructive to investigate the orientations of the copolymers at the interface. The normalised extensions of the end-to-end vector components parallel and perpendicular to the interface of the individual blocks are shown in Fig.16. Right at the interface ( $z = 0$ ) the individual blocks align parallel to the interface, similar to the behaviour of the homopolymers. In the minority phase, the block shrinks, in order to reduce the number of unfavourable interchain contacts. Deep inside the majority phase, the block aligns perpendicular, because the other block pulls it towards the interface. On average, the orientation of individual blocks is however parallel to the interface.

The orientation of the copolymer bonds is shown in Fig.17. The link bonds between the different blocks are strongly oriented perpendicular to the interface. Their orientations increase as the distance from the center of the interface grows. The orientation of the bond vectors, however, rapidly decreases as we approach the ends of the blocks. The bonds in the middle of the blocks behave similar to the bond vectors in homopolymers.

In sum, the shape of a copolymer resembles a dumbbell, the individual blocks are only mildly perturbed and resemble the homopolymer conformations at the interface. The vector, which connects the centers of the distinct blocks, however, has a strong orientation perpendicular to the interface.

The interplay between the interfacial thermodynamics and the phase behaviour of the ternary homopolymer-copolymer mixture is best investigated in the semi-grandcanonical ensemble, which allows the simultaneous measurement of the interfacial free energy and excess quantities. Following Leibler[120], we estimate the chemical potential of the copolymers in the bulk by:

$$N\delta\mu = \ln \rho_c + \frac{1}{2}\chi N, \quad (57)$$

where the first term represents the translational entropy of the copolymer, and the second one the enthalpic repulsion between the homopolymer and the copolymer. The potential of a copolymer adsorbed at the interface, with

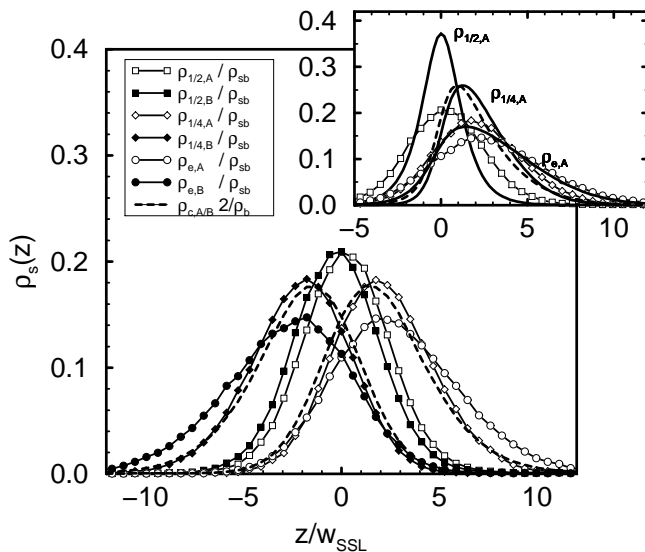


Figure 15: Copolymer segment density profiles for a symmetric diblock copolymer of length 32 at a highly segregated homopolymer interface  $N = 32$  and  $\epsilon = 0.1$ . Apparent profiles are shown for the density of  $A$  and  $B$  monomers in the middle of the chain ( $\rho_{1/2}$ , squares), at the end of the chain ( $\rho_e$ , circles), and at one and three-fourths of the chain ( $\rho_{1/4}$ , diamonds), and for the density of all copolymer monomers ( $\rho_c$ , broken line). The inset shows the predictions of the self-consistent field theory for  $A$  monomers. Full lines show the predictions for segment density profiles  $\rho_{1/2}$ ,  $\rho_e$ , and  $\rho_{1/4}$ , while the broken line presents the total density profile  $\rho_c$ , and symbols compare with the MC results (notation like above). The distance from the interface is measured in units of the predicted width  $w_{SSL}$  in the strong segregation limit and densities are normalised appropriately.

From Ref. [117].

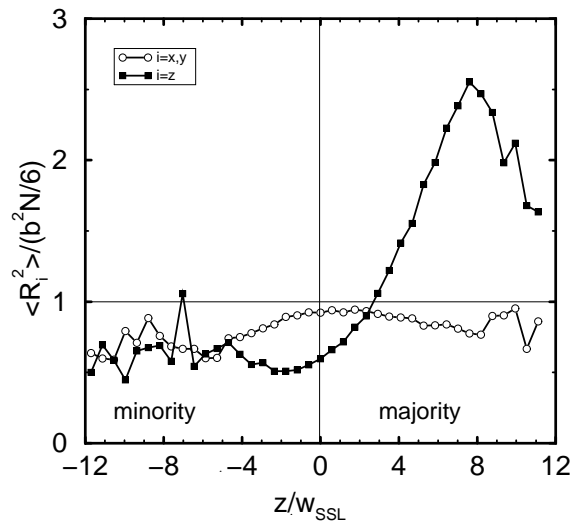


Figure 16: Mean square end-to-end vector components of the copolymer *blocks* in their minority phase (*A* block in *B*-rich phase or vice versa) and majority phase, in units of the average bulk value  $b^2 N / 6$ , plotted as a function of the distance of the midpoint of the end-to-end vector from the interface.

From Ref. [117].

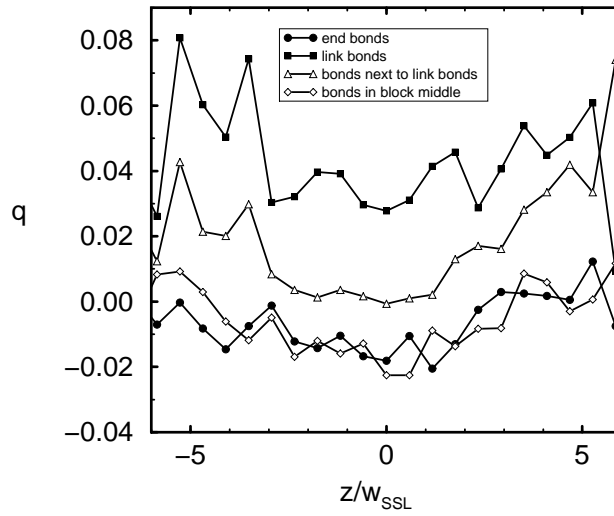


Figure 17: Orientation of bond vectors in a symmetric copolymer of length  $N = 32$  at a highly segregated homopolymer interface ( $\epsilon = 0.1$ ). The orientational order parameter  $q$  for end bonds, link bonds, which join the two blocks, and neighbours of the link bonds are presented. From Ref. [117].

the  $A$  and  $B$  block extended into the appropriate homopolymer regions, is determined by the two-dimensional translational entropy of the joints at the interface,

$$N\delta\mu \approx \ln \frac{\nu N}{\varrho w_C}, \quad (58)$$

where  $w_C$  is the width over which the copolymer joints are confined to the interface, and  $\nu$  is the excess copolymer density at the interface. As shown in the segmental profiles (cf. Fig.15), the width is of the same order than the interfacial width. Semenov[121] has given the estimate  $w_C = \pi w_{\text{SSL}}/2$  for strong segregation. In equilibrium, the chemical potential of the copolymers at the interface and in the bulk are equal, hence

$$\nu \approx \frac{\varrho w_C}{N} \exp\left(\frac{1}{2}\chi N\right). \quad (59)$$

The above considerations neglect the stretching penalty upon crowding copolymers at the interface. This becomes important when the copolymer concentration at the center of the interface is large, *i.e.*,  $\sqrt{6N}\nu/\varrho b \sim \mathcal{O}(1)$ . For higher interfacial excess, the number of copolymers does not increase linearly with the bulk concentration. The dependence of the interfacial enrichment on the bulk concentration for different temperatures is presented in Fig.18 and compared with an analytical expression due to Semenov[121]. The interfacial excess increases upon adding copolymers in the bulk. At low bulk concentrations, we find rather good agreement with the theoretical description, without any adjustable parameter. The saturation at higher copolymer concentrations is described only qualitatively. In this regime of intermediate segregation, the copolymers do not form a well defined stretched brush[75], but rather an unstructured thick layer. Hence the theory overestimates the amount of stretching and the associated entropy loss. This goes along with an underestimation of the copolymer excess.

The adsorption of copolymers also leads to a decrease of the interfacial tension  $\sigma$ . This quantity is directly accessible via the probability distribution of the composition or the Gibbs adsorption isotherm

$$\frac{d\sigma}{k_B T} \approx -\nu_C N \delta\mu, \quad (60)$$

where we have neglected the compressibility of the blend. The results of the direct measurement and the Gibbs adsorption isotherm are presented in Fig.19. Both estimates agree nicely, indicating that the semi-grandcanonical simulation scheme establishes equilibrium between the bulk and the interface[75]. From the slope at vanishing copolymer concentration, we can determine the effective width of the copolymer joint profile  $w_C$ , which agrees rather well with Semenov's estimate  $w_C = \pi w/2$ . In the weak segregation limit, the adsorption of copolymers leads to a compatibilisation of the blend. This

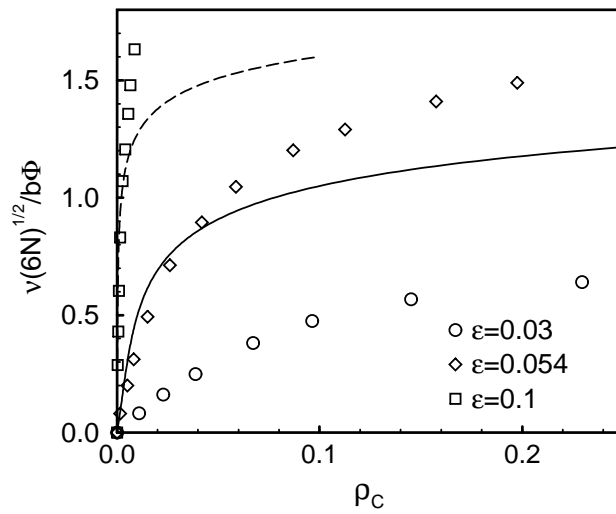


Figure 18: Segregation of symmetric copolymers of length  $N = 32$  at a homopolymer interface. The dependence of the excess areal density  $\nu$  of the copolymers on the bulk concentration is presented for various temperatures. The simulation data are compared without any adjustable parameter to Semenov's theory, which interpolates between the mushroom regime at low  $\nu$  and the brush-like regime for large excess densities. From Ref. [75].

second-order transition is indicated by the arrows in the figure. At higher segregation, we encounter a first order transition at which two homopolymer rich phases coexist with a spatially structured copolymer-rich phase. Both regimes are separated by a tricritical point[75]. The simulations indicate that the spatially structured phase is a swollen lamellar phase at high incompatibilities, and a microemulsion at intermediate incompatibilities. The latter has been established by inspection of the composition correlation functions, which are found to oscillate in space.

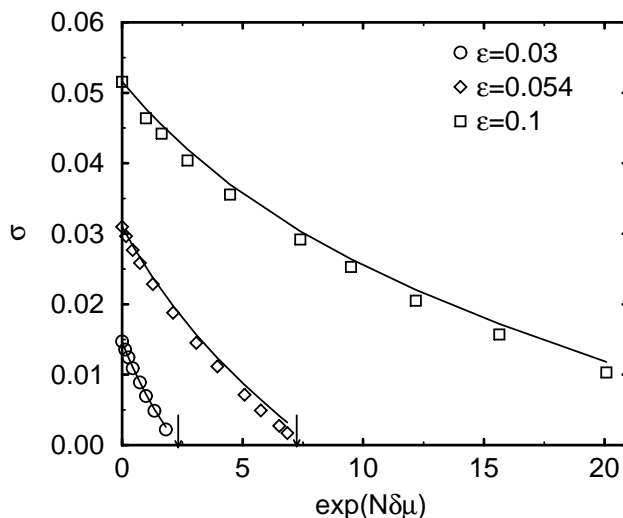


Figure 19: Reduction of the interfacial tension upon increasing the copolymer's chemical potential  $\delta\mu$ . Symbols represent the value of the interfacial tension measured via the reweighting scheme, and lines give the result of the Gibbs isotherm, using the data from the previous figure. The stability limits of the coexisting homopolymer-rich phases are indicated by arrows. Note that the addition of copolymers can reduce the interfacial tension by roughly two orders of magnitude, which is a typical value for amphiphilic systems forming microemulsions. From Ref. [75].

A detailed study of the bulk thermodynamics in the symmetric ternary homopolymer copolymer blend yields a tentative phase diagram over the whole range of copolymer concentrations and incompatibilities (see Fig.20) It includes a two phase region at low copolymer concentration, where two homopolymer-rich phases coexist, and a disordered phase at low incompatibilities and high copolymer concentration. The disordered phase near the

tricritical point (TP) is a microemulsion. A swollen lamellar phase is found at higher incompatibilities and copolymer content. The first order phase transition between the disordered phase and the lamellar phase is indicated by the double solid line. Unfortunately the transition between the microemulsion (DIS) and the (highly defective) lamellar morphology (LAM) could not be located accurately due to the finite simulation box. Hence, the double solid line is just meant schematic. However, the typical snapshots of the morphology also shown in the figure illustrate the qualitative difference between the lamellar phase and the region where a polymeric microemulsion is stable.

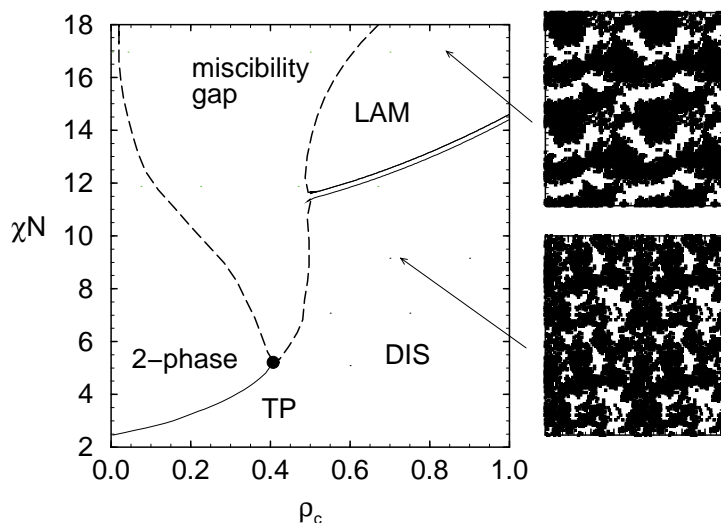


Figure 20: Tentative phase diagram of a symmetric homopolymer-copolymer mixture of chain length  $N = 32$  on the isopleth ( $\Delta\mu = 0$ ). The diagram includes the coexistence between two unstructured homopolymer rich phases (2-phase) and a copolymer-rich disordered phase (DIS) at low incompatibilities. The disordered phase (DIS) is spatially structured (microemulsion) in the vicinity of the triple point (TP). At high incompatibility, we find a strong first order transition (with a large miscibility gap) between two homopolymer-rich phases and a lamellar copolymer-rich phase (LAM). The transition between the disordered phase (DIS, microemulsion) and the lamellar phase could not be located in the simulations, and the double solid lines are meant schematically. Typical snapshots of the  $A$  monomer density in a thin slice through the systems are also presented. For clarity the simulation box ( $L = 80$ ) and three periodic images are shown. The arrows indicate the locations in the phase diagram.

In the weak and strong segregation limit, the simulations agree with self-

consistent field calculations. At intermediate segregation, however, the numerical self-consistent field calculations by Janert and Schick[12] predict the coexistence of two asymmetric highly swollen lamellar phases in the region, where the simulations find a polymeric microemulsion[75]. Furthermore, the self-consistent field calculations predict a multi-critical Lifshitz point instead of a tricritical point.

A discussion of the bending rigidity  $\kappa$  of the interface provides a tentative explanation for the stability of the microemulsion observed in the simulations: At intermediate segregation, the interfacial tension  $\sigma$  becomes very small in the vicinity of the triple line. Thus the bending rigidity controls the interfacial fluctuations, and the persistence length  $\xi_p$  of the interface is of the order  $\xi_p \sim b \exp(2\pi\kappa/k_B T)$  [122]. The bending rigidity of the interface is accessible in the simulations *via* the spectrum of interfacial fluctuations[75] (see Sec. 3). It is presented in Fig.21. The fluctuation spectrum for the pure homopolymer interface is well describable by the capillary-wave Hamiltonian (38) using the independently measured interfacial tension, and this description accounts also rather well for interfaces with a small amount of copolymer adsorbed. Upon increasing the copolymer excess, the interfacial tension decreases, and the deviations from the capillary-wave approximation (40) increase in turn. This indicates that the bending rigidity becomes important, and a satisfactory description of the simulation data is only possible with the full Helfrich Hamiltonian (42). In order to determine the bending rigidity  $\kappa$ , we fit the simulation data to Eqn. (43), fixing the interfacial tension to the value determined via the reweighting scheme. Unfortunately, the bending rigidity cannot be extracted with a high accuracy, yet for our purpose here we only need an order of magnitude estimate. The values of the bending rigidity are small ( $2\pi\kappa/k_B T < 0.5$ ) and increase with growing copolymer concentration. The order of magnitude and the way they depend on the copolymer concentration agree qualitatively with analytical calculations on similar systems[123].

The small value of the bending rigidity of a copolymer-laden interface suggests that interfacial fluctuations destroy the lamellar order predicted by the mean field theory, and lead to the formation of a microemulsion at intermediate segregation. This interpretation is in accord with Monte Carlo simulations of Gompper and Kraus[124], who found that the transition between a microemulsion and a lamellar phase takes place at about  $2\pi\kappa/k_B T \approx 16$ . Note that the chain length  $N = 32$  corresponds to a degree of polymerisation of about 150 on an atomistic level. Our results are thus typical for rather short polymers, and the simulation data exhibit a behaviour between amphiphiles and high molecular weight polymers.

On increasing the chain length  $N$ , the interfacial tension even decreases like  $1/\sqrt{N}$  at constant  $\chi N$ , whereas the bending rigidity  $\kappa$  is expected to grow[125]. Thus  $\kappa$  dominates the fluctuation spectrum in the long chain length limit. De Gennes and Taupin[122] argued that the lamellar phase becomes more favourable for long chain lengths. Therefore, the phase diagram should

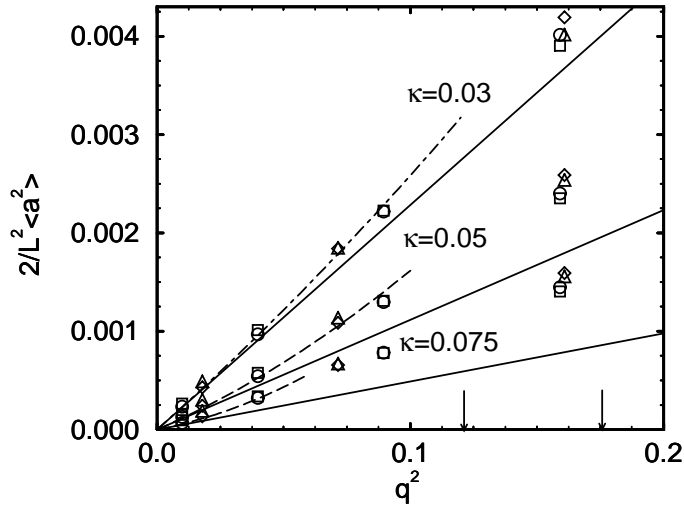


Figure 21: Spectrum of interfacial fluctuations for a symmetric homopolymer-copolymer mixture at  $\epsilon = 0.054$ , *i.e.*, intermediate segregation for three different chemical potentials of the copolymer  $\delta\mu = 0.25, 1.375, 1.75$  from top to bottom. The solid lines shows results of the capillary-wave approximation  $\kappa = 0$  using the independently determined interfacial tension  $\sigma$ . The arrows mark Semenov's estimate for the cutoff  $q_{\max} = 2/w$  for  $\delta\mu = 1.375$  and  $1.75$ . The dashed lines correspond to fits according to the Helfrich Hamiltonian, using the same interfacial tension as before. The fit values of the bending rigidity are indicated. From Ref. [75].

become more mean field like for longer chains. However, in the ultimate vicinity of the tricritical point, both the interfacial tension and the bending rigidity vanish and hence interfacial fluctuations are expected to become important for *all* chain lengths. Indeed, general arguments indicate that isotropic Lifshitz points are unstable in three-dimensional systems [126]. For very long chain lengths, Müller and Schick[75] have speculated that there might be a crossover from Lifshitz tricritical behaviour ( $\xi_p$  large, swollen lamellae) to ordinary tricritical behaviour ( $\xi_p$  small, microemulsion) as one approaches the tricritical point. Recent experiments by Bates et al. [10] found experimental evidence for a bicontinuous polymeric microemulsion in an asymmetric homopolymer copolymer mixture in a region where the self-consistent field theory predicts an isotropic Lifshitz point. In fact, the experimental phase diagram of the copolymer homopolymer mixture closely resembles the phase diagram of small molecule mixtures of oil, water and amphiphiles[127].

#### 4.4 Thin films

The behaviour of confined complex fluid is of practical importance for various applications, *e.g.*, adhesives, coatings, and lubrication. Confining surfaces may alter the phase behaviour profoundly, and the interplay between interfaces separating coexisting bulk-like phases of a binary mixture and the confining walls has attracted longstanding theoretical interest[15, 16, 17].

In the following, we discuss the behaviour of a binary polymer blend, which is confined between two hard, impenetrable walls. Neutral walls, which do not preferentially interact with any of the components, reduce the critical temperature of a symmetric polymer blend and likewise the miscibility gap[128]. This has been investigated through extensive Monte Carlo simulations by Kumar[129] and collaborators, and by Rouault[130] et al. The coexistence curve at the critical point is flattened compared to the bulk binodal, which indicates that the critical point belongs to the 2D Ising universality class. Upon approaching the critical point, the system crosses from mean field to Ising critical behaviour and passes from three-dimensional to two-dimensional critical behaviour.

In general, one component may adsorb preferentially at the surface, such that the wall is coated with a layer of the component with the lower surface free energy. The structural and thermodynamical properties of these wetting layers are of practical importance and of fundamental interest in the statistical mechanics of condensed matter. At phase coexistence of the binary mixture, the surface free energy in the semi-infinite system undergoes a transition, at which the thickness of the adsorbed layer diverges. This wetting transition [15, 16, 17] may be continuous (second-order wetting) or the thickness may jump from a finite value to infinity at the wetting transition temperature. While the unmixing temperature grows linearly with the chain length, the wetting transition in symmetric blends is independent of the chain length. Unlike

the generic situation in mixtures of small molecules, wetting in polymeric systems thus occurs far below the critical point[131]. The wetting behaviour in a binary polymer blend has been studied by Wang[132] and co-workers *via* Monte Carlo simulations in the semi-grandcanonical ensemble.

In a thin film with non-neutral walls, two extreme cases are of special interest: In the asymmetric case, one surface attracts the  $A$  component, whereas the other wall prefers the  $B$  component. In the symmetric situation, both walls attract the same component with equal strength. We discuss their phase behaviour in turn:

In the symmetric situation, the short range potential, which attracts preferentially the  $A$  component, shifts the coexistence chemical potential  $\Delta\mu$  away from its bulk value[128]. At coexistence, the confined system phase separates *laterally* into  $A$  rich domains in coexistence with regions, in which  $A$ -rich layers cover the surfaces, but the  $B$ -component prevails in the center of the film. In the temperature range between the critical temperature of the film and the wetting temperature, the thickness of the wetting layer at coexistence is determined by the interplay of the repulsion between the wall and the  $AB$ -interface, which favours a thick wetting layer, and the shift of the coexistence chemical potential, which suppresses the total amount of the  $A$  component in the film[133]. The semi-grandcanonical ensemble in junction with the reweighting methods permits an accurate location of the coexistence chemical potential, and a good characterisation of the phase behaviour over the whole temperature range. The phase diagram in the bulk, and in a thin film is presented and compared to self-consistent field calculations in Fig. 22[83]. The simulations and the self-consistent field calculations agree qualitatively: The critical temperature is reduced, and at the critical point, the component favoured by the walls is enriched. We find a strong first order wetting transition far below the critical temperature  $T_w \approx 0.2T_c$ . Most notably, the  $A$ -poor binodal is convex in an intermediate temperature regime. This curvature is the signature of the wetting transition in the semi-infinite system.

In the asymmetric case, the effect of the wetting transition is even more fundamental[134, 135]: There always exists at least one interface which runs parallel to the walls and separates an  $A$ -rich phase from a  $B$ -rich one at the appropriate walls. In the temperature regime between the bulk critical temperature and the interface localisation-delocalisation temperature  $T_c(D)$  of a film of width  $D$ , it is localised in the middle of the film. The total composition of this “soft-mode” phase fluctuates around 1/2. Hence, there is no symmetry breaking, and the system is in a one phase region. Below  $T_c(D)$ , two phases coexist in which the interface is localised close to one of the walls. The transition temperature  $T_c(D)$  is smaller than the wetting temperature  $T_w$  of the semi-infinite system, and approaches  $T_w$  exponentially fast as the film thickness  $D$  grows.

In the soft-mode phase, the deviations of the local interfacial position  $u$  from the middle of the film can be described by a capillary-wave Hamiltonian

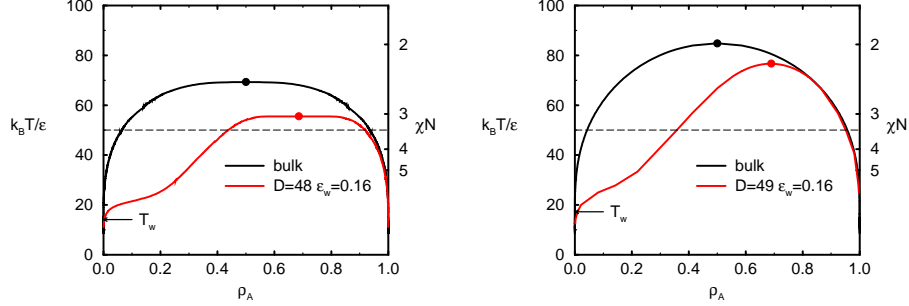


Figure 22: Comparison between the Monte Carlo results (left figure) and the self-consistent field prediction (right diagram) for the phase behaviour of a symmetric, binary polymer blend of chain length  $N = 32$  confined into a thin film of width  $D = 48$  (MC) and  $D = 49$  (SCF). Both surfaces attract the  $A$  component with equal strength  $\epsilon_w = 0.16$ . The wetting temperature of the semi-infinite system is indicated by an arrow. The figures also include the bulk phase diagrams for comparison. From Ref. [83].

(cf. Eqn. 38) augmented by the effective potential exerted by the walls onto the interface. We take the effective interaction between the interface and both walls, which binds the interface to the middle of the film, to be of the form  $V(u) = a(T - T_c(D)) \exp(-\lambda D/2) u^2$ . Here  $1/\lambda$  denotes the effective range of the exponentially decaying potential between the interface and the wall, hence,  $\exp(-\lambda D/2)$  sets the strength of the interaction in the middle of the film. Therefore, the effective Hamiltonian reads

$$\mathcal{H} = \int dx dy \left\{ \frac{\sigma}{2} (\nabla u)^2 + a(T - T_c(D)) \exp(-\lambda D/2) u^2 \right\}. \quad (61)$$

After Fourier decomposing the local interfacial position, we can calculate the spectrum of interfacial fluctuations

$$\frac{2}{L^2 \langle a(q)^2 \rangle} = \frac{\sigma}{k_B T} \left\{ q^2 + \left( \frac{1}{\xi_{\parallel}} \right)^2 \right\}. \quad (62)$$

As in the case of the free interfaces (Eqn. (41)), we integrate the spectrum of capillary waves from  $q_{\min} = 2\pi/L$  to  $q_{\max}$ , and obtain

$$\langle u^2(x, y) \rangle = \frac{k_B T}{2\pi\sigma} \ln \sqrt{\frac{1 + (q_{\max} \xi_{\parallel})^2}{1 + (q_{\min} \xi_{\parallel})^2}}. \quad (63)$$

Note that the parallel correlation length  $\xi_{\parallel}$  plays a similar role than  $q_{\min}$  in

the previous analysis[15]. It is given by

$$\xi_{\parallel} = \frac{1}{\sqrt{\sigma \frac{\partial^2 V}{\partial u^2}}} = \frac{\exp(+\lambda D/4)}{\sqrt{2\sigma a(T - T_c(D))}}. \quad (64)$$

Most notably,  $\xi_{\parallel}$  grows exponentially with the film thickness  $D$ . This is the characteristic signature of the soft mode phase[134]. In a finite system[86],  $\xi_{\parallel}$  can exceed the lateral system dimensions. Depending on whether  $q_{\min}\xi_{\parallel} = 2\pi\xi_{\parallel}/L$  is much larger or much smaller than one, the spectrum is then cut off by the finite lateral system size  $L$ , or by the parallel correlation length  $\xi_{\parallel}$ .

The first limit,  $q_{\min}\xi_{\parallel} \rightarrow \infty$ , corresponds to interfacial fluctuations of a free interface. In the canonical ensemble, the constraint on the composition fixes the laterally averaged position  $\bar{u}$  of the interface and Eqn. (63) can be used to determine the interfacial width. In the semi-grandcanonical ensemble, the average position of the interface is unconstrained, and one has an additional  $q = 0$ -mode, which corresponds to a translation of the interface as a whole, and which dominates the broadening. With the effective Hamiltonian (61), the fluctuations of the average interfacial position are then given by  $\langle \bar{u}^2 \rangle = k_B T \xi_{\parallel}^2 / (L^2 \sigma)$ . In the limit  $L \ll \xi_{\parallel}$ , the fluctuations are of the order  $D^2$  itself, and thus  $w = D/2$  in the semi-grandcanonical ensemble.

In the second limit,  $q_{\min}\xi_{\parallel} \rightarrow 0$ , the dependence of the parallel correlation length on the film thickness leads to an anomalous size dependence[137, 86] of the apparent interfacial width. Using the convolution approximation (46) and the above equation for the lateral correlation length, we get

$$w^2 \approx w_0^2 + \frac{k_B T}{4\sigma} \ln q_{\max}\xi_{\parallel} = w_0^2 + \frac{k_B T \lambda D}{16\sigma} + \text{const.} \quad (65)$$

Hence, the width of the apparent profiles increases like  $\sqrt{D}$  for large lateral extensions. The dramatic dependence on the film thickness demonstrates the importance of careful assessment of interfacial fluctuations, when analysing apparent interfacial profiles. This finding is also relevant to interfaces in mixtures of small molecules, and in particular to the interpretation of experimental data[138]. In the symmetric case (capillary condensation) or in the presence of long ranged (van der Waals) interactions, the dependence of the interfacial width on the film width  $D$  is, however, only logarithmic.

The structure and profiles across the film in the soft-mode phase have been studied with extensive Monte Carlo simulations by Werner et al.[86]. The system considered is a symmetric, binary blend of polymers with chain length  $N_A = N_B = 32$ , confined to a thin film of width  $D$ . The left surface attracts  $A$  monomers, which are less than 2 lattice spacings away, and repels  $B$  monomers, with an interaction of strength  $\epsilon_w = 0.1$ . Likewise, the right surface prefers  $B$  monomers and repels  $A$  segments. The temperature  $1/\epsilon = 33.3$  was chosen higher than the wetting temperature in the semi-infinite geometry, hence the system is without doubt in the soft-mode phase. In Fig. 23, the

apparent interfacial width  $w$  is shown as a function of the film thickness  $D$  for very large lateral system size  $L = 256$  in the semi-grandcanonical ensemble. The large lateral system extension ensures, that the fluctuation spectrum is cut off by the parallel correlation length  $\xi_{\parallel}$ . The Monte Carlo data are compared to the prediction (65), where the range of the interfacial interaction  $\lambda$  is taken to be  $1/\lambda = \xi(1 + k_B T/8\pi\xi^2\sigma)$ [135, 136] with the bulk correlation length  $\xi$ , and the constant term is taken to be zero. Both, the bulk correlation length and the interfacial tension have been measured independently. The intrinsic width has been extracted from a self-consistent field calculation in an infinite system[52]. The Monte Carlo data and the predictions agree nicely for thick films; however, there are deviations for very thin films. This can be understood from the following consideration: If the film width  $D$  is not very much larger than the radius of gyration  $R_g(N = 32) \approx 7$ , the intrinsic profile  $\rho_0$  is squeezed. Such an effect has been observed in simulations[86] and in self-consistent field calculations[83]. It can be analysed *via* a block analysis (see Sec. 3) by inspection of the width of the reduced profiles as a function of the block size  $B$ . If  $B$  is larger than the short wavelength cut-off of the interfacial fluctuation spectrum  $1/q_{\max}$ , the reduced profiles are broadened by capillary waves. One can attempt to identify an effective intrinsic width with the value  $w_0(D)$  attained at the subsystem size  $B = 8 \approx R_g$ . As shown in Fig. 24, Eqn.(65) in combination with this effective width  $w_0(D)$  quantitatively accounts for the deviations at small film thicknesses.

The relationship between the width of the apparent interfacial profiles and the film thickness follows from general considerations on the statistical mechanics of interfaces, and is not restricted to polymeric systems. Similar effects have been observed previously in simulations of simple Ising models[137]. However, polymer blends are particularly suited for investigating phenomenological concepts of surface enrichment, wetting, interfacial localisation-delocalisation transitions and capillary condensation, because the chain length  $N$  constitutes an additional control parameter[131]. On increasing the chain length  $N$ , one can reduce bulk composition fluctuations, which are ignored in most phenomenological approaches. There exist powerful analytical tools to describe the bulk and interfacial behaviour in the long chain length limit. In addition, the phenomena occur on larger length scales due to the large size of the polymer coils, which facilitates applications of several experimental techniques. In fact, the anomalous size dependence of the apparent interfacial width has first been observed experimentally in a polymer system by Kerle et al.[138].

## 5 Conclusions and outlook

We have reviewed extensive computer simulations on the bulk thermodynamics and interfacial structure of polymer blends in the melt state. Simulations of polymer blends and interfaces are considerably more exacting in computa-

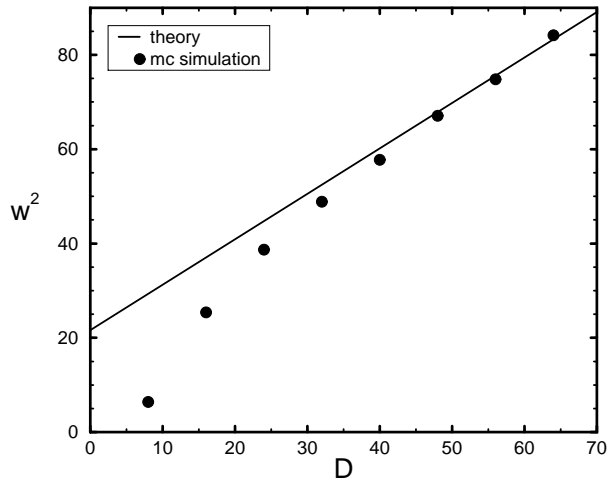


Figure 23: Monte Carlo results for the apparent interfacial profile width of a symmetric, binary polymer blend  $N = 32$  in a thin film of thickness  $D$ . The confining surfaces attract different components of the blend with an interaction potential  $\epsilon_w = 0.1$ . The temperature  $\epsilon = 0.03$  is well above the wetting temperature. Shown is the squared interfacial width  $w^2$  as a function of the film thickness  $D$  for large lateral system extension  $L = 256$ . The straight line shows the expected a capillary-wave broadening, when the interfacial fluctuation spectrum is cut off by the thickness dependent parallel correlation length  $\xi_{||}$ . From Ref. [86].

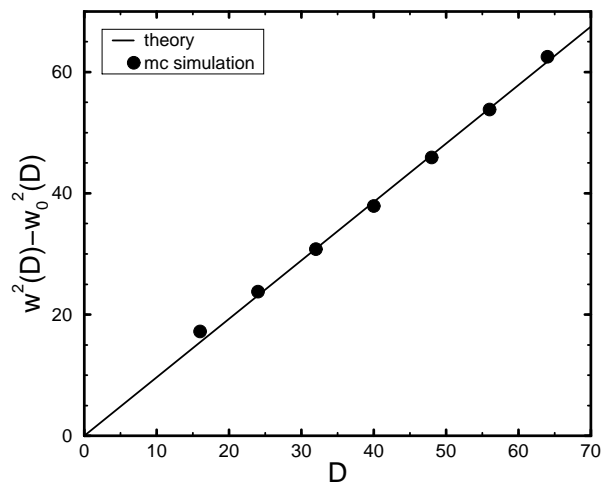


Figure 24: Same data as in the previous figure, but the squeezing of the intrinsic interfacial width due to the confining surfaces is accounted for by subtracting the estimated intrinsic width  $w_0^2(D)$ . The straight line corresponds to the expected capillary-wave broadening. From Ref. [86].

tional terms than those of small molecular fluids or magnetic systems. The difficulties stem from the difficulty of dealing with the widely spread time and length scales caused by the extended structure of the macromolecules. The accurate determination of the macroscopic behaviour while retaining the detailed atomistic chemical structure is not feasible even with state-of-the-art supercomputers. Yet, by a careful choice of the statistical ensemble, use of recently developed simulation techniques and sophisticated data analysis methods, simulations of coarse-grained polymer models yield valuable insight into the structural and thermodynamic properties of polymeric composites.

Simulations contribute to the identification of important effective parameters, which determine qualitatively the bulk and interfacial properties. They can examine the influence of the coarse-grained chain architecture on the phase and interfacial behaviour. As an example, we have discussed how stiffness disparity[46] between the components gives rise to a positive contribution to the Flory-Huggins parameter  $\chi$ . This finding is in agreement with field theoretical considerations[38] and P-RISM calculations[37]. Furthermore, we have shown that the persistence length affects the interfacial behaviour in highly incompatible blends. For weak incompatibilities, the effect of the stiffness can be modelled within the Gaussian chain model. This model incorporates two parameters, the incompatibility  $\chi N$ , and the length scale  $R$  set by the polymer radius of gyration. In the strong segregation limit, the width of the interface scales as  $R/\sqrt{\chi N}$ . However, for large incompatibilities the interfacial width becomes of the order of the persistence length. On this length scale, the conformations are not Gaussian, but the bond vectors are strongly correlated. In this regime simulations and self-consistent field calculations show that the interfacial width decreases upon increasing the stiffness disparity, in qualitative contrast[53] to the predictions of the Gaussian chain model.

Many static and dynamical properties on various length scales are simultaneously accessible in simulations. Therefore the simulations provide a detailed picture of the interfacial properties in binary and ternary polymer mixtures. Both structural informations (*e.g.*, the orientation of bond vectors, or of whole chains[51, 52, 117], the adsorption of copolymers[75], the enrichment of vacancies) as well as thermodynamic properties (*e.g.*, the interfacial tension or the bending rigidity) are obtained simultaneously and hence permit a quantitative comparison with other theoretical approaches like scaling descriptions[1], self-consistent field calculations[21, 22, 23, 24], density functional theories[25, 101] and P-RISM calculations[31].

Simulations of the interfacial behaviour of symmetric block copolymers[117] yield a detailed picture of the structure. If the areal density of copolymers adsorbed at the homopolymer interface is small, the copolymers assume dumbbell-like conformations. The individual blocks extend into the appropriate bulk phases and resemble only mildly perturbed homopolymers, in particular each block is aligned parallel to the interface. This finding is in

qualitative agreement with available experimental data by Russell et al.[119].

In general, simulations and mean field treatments agree qualitatively, because the extended structure of the polymers suppresses fluctuations, and microscopic details can be qualitatively described with a few effective, coarse-grained parameters. The simulation can access the way in which the mean field behaviour is approached upon increasing the chain length[49]. However, one important source of discrepancy between simulations and mean field theories are interfacial fluctuations and we have highlighted two consequences:

In ternary homopolymer copolymer blends[75], interfacial fluctuations destroy the order in highly swollen lamellar phases and lead to the fluctuation-induced formation of a microemulsion. Simulations find tentative evidence for a tricritical point, where the mean field treatment[12] predicts a Lifshitz tricritical point in symmetric systems. Upon increasing the chain length, however, there may be a crossover from Lifshitz criticality to ordinary tricritical behaviour[75]. This “catastrophic failure of mean-field theory”[10] is also observed in recent experimental studies by Bates and coworkers. These experiments on an asymmetric ternary blend find a bicontinuous microemulsion close to the region, where the mean-field treatment predicts an isotropic Lifshitz point. The mesoscopic structured yet macroscopic homogeneous composites possibly have unique and useful mechanical or electrical materials properties[10].

Interfacial fluctuations profoundly influence apparent profiles measured in simulations[86]. They lead to a pronounced broadening of the width of the measured profiles. In a thin film with asymmetric surfaces attracting different components, there exists a temperature regime[134], in which one interface separating an  $A$  rich domain and a  $B$  rich one runs parallel to the surfaces in the middle of the film. Effective interactions between the interface and both walls pin this interface to the middle of the film, and generate a parallel correlation length  $\xi_{\parallel}$  which grows exponentially with the film thickness  $D$  in the case of short range interactions. This large length scale acts as a cut-off for the spectrum of capillary waves, and consequently limits the broadening. The apparent interfacial width increases like  $\sqrt{D}$ . If we were to include long range van der Waals interaction in our simulations, we would expect a logarithmic dependence of the apparent interfacial width on the film thickness. The effect is also pertinent to the interpretation of recent experimental studies[138, 139, 140].

In view of these findings, it would be of interest in future simulation studies to investigate the role of the short length scale cut-off of the interfacial fluctuations spectrum. A study of the way how the capillary-wave broadening depends on the chain length, and on the incompatibility, might help to solve the question, whether and how the length scales of the lateral fluctuations contributing to the intrinsic profile or to the capillary-wave broadening can be separated from each other. This might contribute in general to the interpretation of intrinsic profiles calculated in analytical approaches. Another,

more subtle point, concerns the way the *shape* of the profiles is affected by the capillary-wave broadening. The intrinsic profiles obtained, *e.g.*, with a block analysis, should be reasonably well described by a tanh profile, at least in the weak segregation limit. Preliminary results indicate that the intrinsic profiles are indeed closer to a tanh shape than to an error function shape as the critical point is approached[140]. The shape of the apparent profiles is given by the convolution of the intrinsic profile and the gaussian curve associated with the capillary broadening, which is closer to an error function in large enough systems. The latter error function shape has been established for the case of capillary-wave broadening in Ising models only recently by Moseley[141].

Moreover, the dynamical evolution of interfacial profiles, after two flat interfaces have been brought into contact, is relevant in some experimental situations. Simulations might investigate whether there is a separation of time scales on which an intrinsic profile develops which is then, on a different time scale, broadened by capillary waves.

A few other interesting questions shall be sketched briefly: The interfacial properties of random or branched copolymers have attracted considerable interest because of the extensive commercial applications. Recent interest stems from experimental progress of the reactive polymer blending techniques[142]. This has been subsequently studied theoretically[143, 144, 145, 146] for rather idealised situations. Other important problems are related to the single chain dynamics in blends. In the miscible case, *e.g.*, simulations could test recent theoretical predictions by Schweizer[147] and co-workers on the coupling between the thermodynamics and the single chain dynamics.

Furthermore, recent attempts to construct even more coarse-grained model[148], which incorporate the instantaneous shape of a polymer only *via* a continuous distribution of its monomer density, might offer promising routes to investigate the large length scale properties of macromolecular composites. This might shed some light onto the mechanical properties of polymeric interfaces, which are of long standing practical and experimental interest.

## Acknowledgements

It is a great pleasure to thank K. Binder, M. Schick, N.B. Wilding, A. Werner and P. Janert for enjoyable and fruitful collaborations and many stimulating discussions, and K. Binder and A. Werner in particular for a critical reading of this manuscript. Financial support by the grants DFG Bi 314/3-4, BMBF 03N8008C, NSF DMR9220733 and the Alexander von Humboldt foundation are gratefully acknowledged, as well as generous grants of computing time at the computing centers CINECA (Bologna, Italy), EPFL (Lausanne, Suisse), SDSC (San Diego, USA), the Johannes Gutenberg university (Mainz, Germany), HLRZ (Juelich, Germany), and RUS (Stuttgart, Germany).

## References

- [1] P. G. de Gennes, *Scaling Concepts in Polymer Physics* (Cornell University Press, Ithaca, New York, 1979).
- [2] G. I. Taylor, *Proc. R. Soc. London, Ser. A* 138, 41(1932).
- [3] S. Wu, *Polym.Eng.Sci.* 27, 335(1987).
- [4] F. S. Bates, G. H. Fredrickson, *Ann. Rev. Phys. Chem.* 41, 512(1990).
- [5] S. H. Anastasiadis, I. Gancarz, J. T. Koberstein, *Macromolecules* 22, 1449(1989).
- [6] N. C. Beck Tan, S.-K. Tai, R.M. Briber, *Polymer* 37, 3509(1997).
- [7] S. T. Milner, H. Xi, *J. Rheology* 40, 663 (1996); S. T. Milner, *MRS Bulletin* 22, 38(1997).
- [8] H. R. Brown, V. R. Deline, P. F. Green, *Nature* 341, 221(1989); *Macromolecules* 26, 4155(1993); H. R. Brown, *Macromolecules* 22, 2859(1989).
- [9] D. J. Kinning, K. I. Winey, E. L. Thomas, *Macromolecules* 21, 3502(1988); D. J. Kinning, *J. Chem. Phys.* 90, 5806 (1989); K. I. Winey, E. L. Thomas, L. J. Fetters, *J. Chem. Phys.* 90, 9367(1991);
- [10] F. S. Bates, W. W. Maurer, P. M. Lipic, P. M. A. Hillmyer, K. Almdal, K. Mortensen, G. H. Fredrickson, T. P. Lodge, *Phys. Rev. Lett.* 79, 849(1997).
- [11] L. Leibler, P. A. Pincus, *Macromolecules* 17, 2922(1984); A. N. Semenov, *Macromolecules* 26, 2273(1993); M. W. Matsen, F. S. Bates, *Macromolecules* 29, 1091 (1996).
- [12] P. K. Janert, M. Schick, *Macromolecules* 30, 3916(1997); P. K. Janert, M. Schick, *Macromolecules* 30, 137(1997).
- [13] M. Templin, A. Franck, U. Chesne, H. Leist, Y. Zhang, R. Ulrich, V. Schädler, U. Wisner, *Science* 278, 1795 (1997).
- [14] F.S. Bates, *Science* 251, 898 (1991).
- [15] M. Schick, *Les Houches lectures on "Liquids at interfaces"*, Elsevier Science Publishers B.V. (1990); S. Dietrich, in *Phase Transitions and Critical Phenomena*, Vol. 12, C. Domb and J.L. Lebowitz (eds) NY Academic Press (1988).
- [16] P. G. de Gennes, *Rev. Mod. Phys.* 57, 827(1985);

- [17] A. O. Parry, J. Phys.: Cond. Matt. 8, 10761(1996); R. Evans, J.Phys.:Cond.Matt. 2, 8989 (1990); R. Evans, U. Marini, B. Marconi, P. Tarazona, J.Chem.Phys. 84, 2376 (1986).
- [18] V. L. Ginzburg, Sov. Phys. Solid state 1, 1824(1960); P.-G. de Gennes, J. Phys. Lett. (Paris) 38, L-441(1977); J. F. Joanny, J. Phys. A 11, L-117(1978); K. Binder, Phys. Rev. A 29, 341(1984).
- [19] For a recent review, see R. Holyst, T. A. Vilgis, Macromol. Theory and Simulations 5, 573(1996).
- [20] S. G. Glotzer, in *Annual Reviews of Computational Physics II*, p. 1, World Scientific, Singapore (1995).
- [21] E. Helfand, Y. Tagami, J. Polym. Sci. B 9, 741(1971); J. Chem. Phys. 56, 3592(1971); 57, 1812(1972); E. Helfand, A. M. Sapse, J. Chem. Phys. 62, 1327(1975); E. Helfand, J. Chem. Phys. 62, 999 (1975).
- [22] J. Noolandi, K. M. Hong, Macromolecules 14, 727(1981); 15, 483(1982);
- [23] K. R. Shull, Macromolecules 26, 2346(1993); K. R. Shull, E. J. Kramer, Macromolecules 23, 4769(1990).
- [24] J. M. H. M. Scheutjens, G. J. Fleer, J. Chem. Phys. 83, 1619(1979); D. N. Theodourou, Macromolecules 22, 4578(1989).
- [25] H. Tang, K. F. Freed, J. Chem. Phys. 94, 1572(1991); K. F. Freed, J. Chem. Phys. 103, 3230(1995).
- [26] P.J. Flory, J. Chem. Phys. 9, 660(1941); H. L. Huggins, J. Chem. Phys. 9, 440(1941).
- [27] P. Flory, *Principles of Polymer Chemistry* (Cornell University Press, Ithaca, New York, 1971).
- [28] A. I. Pesci, K. F. Freed, J. Chem. Phys. 90, 2003 and 2017(1989); J. Dudowicz, K. F. Freed, Macromolecules 24, 5076, 5096 and 5112(1991); K. W. Foreman, K. F. Freed, I. M. Ngola, J. Chem. Phys. 107, 4688(1997).
- [29] J. Dudowicz and K. F. Freed, Macromolecules 23, 1519(1990); M. Lifschitz and K. F. Freed, J. Chem. Phys. 98, 8994(1993). K. W. Foreman and K. F. Freed, J. Chem. Phys. 102, 4663(1995).
- [30] F. Aguilera-Granja, R. Kikuchi, Physica A 176, 514(1990); 182, 331(1991); 189, 81 (1992); 189, 108(1992).
- [31] For a recent review, see K. S. Schweizer, J. G. Curro, in *Advances in Chemical Physics*, Vol XCVIII, I. Prigogine and S. A. Rice (eds.), Wiley, New York(1997).

- [32] C. J. Grayce, K. S. Schweizer, *J. Chem. Phys.* 100, 6846(1994); C. J. Grayce, A. Yethiraj, K.S. Schweizer, *J. Chem. Phys.* 100, 6857(1994).
- [33] *Monte Carlo and Molecular Dynamics Simulations in Polymer Science*, K. Binder ed., Oxford University Press, New York (1995).
- [34] T. B. Liverpool, in *Annual Reviews of Computational Physics IV*, p. 317, World Scientific, Singapore (1996).
- [35] K.F. Freed, *Renormalization Group Theory of Macromolecules*, Wiley-Interscience, NY(1987).
- [36] J. H. Hildebrand, R. L. Scott, *The solubility of non-electrolytes*, Dover, New York, (1964).
- [37] C. Singh, K. S. Schweizer, *J. Chem. Phys.* 103, 5814(1995); C. Singh, K. S. Schweizer, *Macromolecules* 30, 1490(1997);
- [38] G. H. Fredrickson, A. J. Liu, F.S. Bates, *Macromolecules* 27, 2503(1994).
- [39] J. Higgins, H. Benoit, *Polymers an Neutron Scattering*, (Oxford University Press, New York, 1994).
- [40] F. S. Bates, M. Muthukumar, G. D. Wignall, L. J. Fetters, *J. Chem. Phys.* 89, 535(1988); J. D. Londono, A. H. Narten, G. D. Wignall, K. G. Honnell, E. T. Hsieh, T. W. Johnson, F. S. Bates, *Macromolecules* 27, 2864(1994).
- [41] R. Krishnamoorti, W. W. Graessley, N. P. Balsara, D. J. Lohse, *J. Chem. Phys.* 100, 3894(1994).
- [42] J. K. Taylor, P. G. Debenedetti, W. W. Graessley, S. K. Kumar, *Macromolecules* 29, 764(1996).
- [43] S. K. Kumar, B. A. Veytsman, J. K. Maranas, B. Crist, *Phys. Rev. Lett.* 79, 2265(1997).
- [44] R. Holyst and T.A. Vilgis, *Phys.Rev. E* 50, 2087 (1994).
- [45] J. D. Weinhold, S. K. Kumar, C. Singh, K. S. Schweizer, *J. Chem. Phys.* 103, 9460(1995).
- [46] M. Müller, *Macromolecules* 28, 6556(1995).
- [47] G. S. Grest, M. D. Lacasse, K. Kremer, A.M. Gupta, *J. Chem. Phys.* 105, 10583(1996); G. S. Grest, M. D. Lacasse, M. Murat, *MRS Bulletin* 22, 27(1997).
- [48] H.-P. Deutsch, K. Binder, *Europhys. Lett.* 17, 697(1992); H.-P. Deutsch, K. Binder, *Macromolecules* 25, 6214(1992).

- [49] M. Müller, K. Binder, *Macromolecules* 28, 1825(1995).
- [50] K. S. Schweizer, *Macromolecules* 26, 6033(1993) *ibid* 6050(1993); K. S. Schweizer, *J. Chem. Phys.* 98, 9053(1993) *ibid* 9080(1993).
- [51] M. Müller, K. Binder, W. Oed, *Faraday Trans.* 91, 3269(1995).
- [52] F. Schmid and M. Müller, *Macromolecules* 28, 8639(1995).
- [53] M. Müller, A. Werner, *J. Chem. Phys.* 107, 10764(1997).
- [54] F. Schmid, *J. Chem. Phys.* 104, 9191(1996).
- [55] J.-P. Hansen, I.R. McDonald, *Theory of simple liquids*, Academic Press, London (1990).
- [56] A. Yethiraj, K. S. Schweizer, *J. Chem. Phys.* 98, 9053(1993).
- [57] K. Binder, *Adv. Poly. Sci.* 112 181(1994).
- [58] K. Binder, *Adv. Poly. Sci.* in press (1998).
- [59] K. Binder, *Acta Polymer* 46, 204(1995).
- [60] H. Gehlsen, J. Rosedale, F. S. Bates, G. Wignall, L. Hansen, K. Almdal, *Phys. Rev. Lett.* 68, 2452(1992).
- [61] H.-P. Deutsch, *J. Stat. Phys.* 67, 1039(1992).
- [62] A. Yethiraj, R. Dickman, *J. Chem. Phys.* 97, 4468(1992).
- [63] I. Carmesin, K. Kremer, *Macromolecules* 21, 2819(1988); H.-P. Deutsch, K. Binder, *J. Chem. Phys.* 94, 2294(1991).
- [64] W. Paul, K. Binder, D. W. Heermann, K. Kremer, *J. Chem. Phys.* 95, 7726(1991).
- [65] V. Tries, W. Paul, J. Baschnagel, K. Binder, *J. Chem. Phys.* 106, 738(1997); W. Paul, N. Pistor, *Macromolecules* 27, 1249(1994); W. Paul, K. Binder, J. Batoulis, B. Pittel, K. H. Sommer, *Makromol. Chem., Macromol.Symp.* 64, 1(1993).
- [66] P. Doruker and W. L. Mattice, *Macromolecules* 30, 5520(1997).
- [67] N. B. Wilding, M. Müller, K. Binder, *J. Chem. Phys.* 105, 802(1996).
- [68] M. Müller, J. P. Wittmer, M. E. Cates, *Phys. Rev. E* 53, 5069(1996).
- [69] J. Baschnagel, K. Binder, *Macromolecules* 28, 6808(1995).

- [70] G. Y. A. Ypma, P. Cifra, E. Nies, A. R. D. vanBergen, *Macromolecules* 29, 1252(1996); P. Cifra, E. Nies, F. E. Karasz, *Macromolecules* 27, 1166(1994).
- [71] R. B. Pandey, A. Milchev, K. Binder, *Macromolecules* 29, 1194(1997).
- [72] P. Wiltzius, F. S. Bates, *J. Chem. Phys.* 91, 3258(1989); H. Tanaka, *Phys. Rev. Lett.* 71, 3158 (1993); J. S. Langer, M. Bar-on, H. D. Miller, *Phys. Rev. A* 11, 1417(1975).
- [73] M. Müller, K. Binder, *Comp.Phys.Comm.* 84, 173 (1994).
- [74] A. Sariban, K. Binder, *Macromolecules* 21, 711 (1988); A. Sariban, K. Binder, *J.Chem.Phys.* 86, 5859 (1987).
- [75] M. Müller, M. Schick, *J. Chem. Phys.* 105, 8885(1996).
- [76] H.-P. Deutsch, *J.Chem.Phys.* 99, 4825 (1993).
- [77] M. Rovere, D.W. Heermann, K. Binder, *Europhys.Lett.* 6, 585 (1988); *J.Phys.: Condensed Matter* 2, 7009 (1990).
- [78] M. Müller, N. B. Wilding, *Phys. Rev. E* 51, 2079(1995).
- [79] N. B. Wilding, *Phys. Rev. E* 52, 602(1995); N. B. Wilding, *J. Cond. Matter* 9, 585(1997).
- [80] A. M. Ferrenberg, R. H. Swendson, *Phys. Rev. Lett.* 61, 2635(1989); *ibid.* 63, 1195(1989); J. Bennett, *J. Comput. Phys.* 22, 245(1979).
- [81] B. A. Berg, T. Neuhaus, *Phys. Rev. Lett.* 68, 9(1992).
- [82] K. Binder, *Phys.Rev A* 25, 1699(1982).
- [83] M. Müller, K. Binder, preprint December 1997.
- [84] M. Müller, *EPFL Supercomputer Review* 7, 21(1995).
- [85] M. Müller, M. Schick, *J. Chem. Phys.* 105, 8282(1996).
- [86] A. Werner, F. Schmid, M. Müller, K. Binder, *J. Chem. Phys.* 107, 8175(1997).
- [87] F. P. Buff, R. A. Lovett, F. H. Stillinger, *Phys. Rev. Lett.* 15, 621(1965).
- [88] W. Helfrich, *Z. Naturforsch.* 28c, 693(1973); P. B. Canham, *J. Teor. Biol.* 26, 61(1970). E. Evans, *Biophys. J.* 14, 923(1974).
- [89] A. N. Semenov, *Macromolecules* 26, 6617(1993); 27, 2732(1994).
- [90] D. Jasnov, *Rep. Prog. Phys.* 47, 1059 (1984).

- [91] F. Scheffold, E. Eiser, A. Budkowski, U. Steier, J. Klein, L. J. Fetters, J. Chem. Phys. 104, 8786 and 8796(1996).
- [92] F. S. Bates, I. H. Rosedale, P. Stepanek, T. P. Lodge, P. Wiltzius, G. H. Fredrickson, R. P. Hjelm, Phys. Rev. Lett. 65, 1839(1990); D. Schwahn, S. Janssen, T. Springer, J. Chem. Phys. 97, 8775(1992); D. W. Hair, E. K. Hobbie, J. Douglas, C. C. Han, Phys. Rev. Lett. 68, 2476(1992).
- [93] J.D. Honeycutt, Macromolecules 27, 5377(1994).
- [94] D. Schwahn, K. Mortensen, T. Springer, H. Yee-Madeira, R. Thomas, J. Chem. Phys. 87, 6078(1987).
- [95] R. Dickman Comput. Polym. Sci. 1, 206(1991).
- [96] S. K. Kumar, Macromolecules 27, 260(1994); 30, 5085(1997).
- [97] S. K. Kumar, J. D. Weinhold, Phys. Rev. Lett. 77, 1512(1996).
- [98] R. Holyst, T.A. Vilgis, J. Chem. Phys. 99, 4835(1993).
- [99] D. C. Morse, G. H. Fredrickson, Phys. Rev. Lett. 73, 3235(1994).
- [100] N. Saito, K. Takahashi, Y. Yunoki, J. Phys. Soc. Jpn. 22, 219(1967).
- [101] H. Tang, K. F. Freed, J. Chem. 94, 6307(1991).
- [102] A. V. Ermoshkin, A. N Semenov, Macromolecules 29, 6294(1996); A. N. Semenov, J. Phys. II 6, 1759(1997).
- [103] see, *e.g.*, *Physics of Polymer Surfaces and Interfaces*, ed. I.C. Sanchez, Butterworth-Heinemann, Boston(1992).
- [104] T. P. Russell, Materials Science Reports 5, 171(1990).
- [105] T. Nose, T. Tanabe, Macromolecules 30, 5457(1997).
- [106] M. Stamm, D. W. Schubert, Ann. Rev. Mat. Sci 25, 326(1995); D. W. Schubert, V. Abetz, M. Stamm, T. Hack, W. Siol, Macromolecules 28, 2519(1995).
- [107] B. Löwenhaupt, G. P. Hellmann, Colloid & Polymer Sci. 268, 885(1990).
- [108] H. E. Hermes, J. S. Higgins, D. G. Bucknall, Polymer 38, 985(1997).
- [109] K. H. Dai, E. J. Kramer, Polymer 35, 157(1994); *ibid* Macromolecules 25, 220(1992).
- [110] J. Reiter, G. Zifferer, O. F. Olaj, Macromolecules 23, 224(1990).
- [111] M. D. Lacasse, G. S. Grest, A.J. Levine, Phys. Rev. Lett. 80, 309(1998).

- [112] Y. Wang, W. L. Mattice, J. Chem. Phys. 98, 9881(1993); Y. Wang, Y. Li, W. L. Mattice, J. Chem. Phys. 99, 4068 (1993); A. C. Balasz, D. Gersappe, R. Israels, M. Fasolera, Makrom. Theory Simul. 4, 585 (1995).
- [113] J.-U. Sommer, G. Peng, A. Blumen, J. Physique II 6, 1061 (1996); J. Chem. Phys. 105, 8376 (1996).
- [114] T. Pan, K. Huang, A. C. Balasz, M. S. Kunz, A. M. Mayes, T. P. Russell, Macromolecules 26, 2860(1993).
- [115] E. Helfand, S. M. Bhattacharjee, G. H. Fredrickson, J. Chem. Phys. 91, 7200(1989).
- [116] D. Broseta, G. H. Fredrickson, E. Helfand, L. Leibler, Macromolecules 23, 132(1990).
- [117] A. Werner, F. Schmid, K. Binder, M. Müller, Macromolecules 29, 9241(1996).
- [118] C. Creton, E.J. Kramer, G. Hadziioannou, Macromolecules 24, 1846(1991); J. Washiyama, C. Creton, E. J. Kramer, Macromolecules 25, 4751(1992); E. J. Kramer, Adv. Polym. Sci. 52/53, 1(1983).
- [119] P. F. Green, T. P. Russell, Macromolecules 24 2931(1991); K. R. Shull, A. M. Mayes, T. P. Russell, Macromolecules 26 3929(1993).
- [120] L. Leibler, Makromol. Chem. Macromol. Symp. 16, 1(1988); Physica A 172, 258(1991).
- [121] A. N. Semenov, Macromolecules 25, 4967(1992).
- [122] C. Taupin, P.G. deGennes, J. Phys. Chem. 86, 2294(1982).
- [123] M. W. Matsen, M. Schick, Macromolecules 26, 3878(1993); *ibid* 27, 2317(1994).
- [124] G. Gompper, M. Kraus, Phys. Rev. E 47, 4289 and 4301(1993).
- [125] R. Cantor, Macromolecules 14, 1186(1981). Z. G. Wang, S. A. Safran, J. Phys. France 51, 185(1990).
- [126] N. S Tonchev, D. I. Uzunov, Physica A 134, 265(1985); O. V. Vasilev, K. A. Dawson, Phys. Rev. E 50, 2115(1994); R. M. Hornreich et al., Z.Phys. B 35, 91(1979); A. Erzan, G. Stell, Phys. Rev. B 16, 4146 (1977).
- [127] M. C. Barbosa, M. Frichebruder, Phys. Rev. 51, 4690(1995).
- [128] M. E. Fisher, H. Nakanishi, J. Chem. Phys. 75, 5857(1981); H. Nakanishi, M. E. Fisher, J. Chem. Phys. 78, 3279 (1983).

- [129] S. K. Kumar, H. Tang, I. Szleifer, *Mol.Phys.* 81, 867(1994).
- [130] Y. Rouault, J. Baschnagel, K. Binder, *J. Stat. Phys.* 80, 1009(1995); Y. Rouault, B. Dünweg, J. Baschnagel, K. Binder, *Polymer* 37, 297(1996).
- [131] I. Schmidt, K. Binder, *J. Phys.* 46, 1631(1985); H. Nakanishi, P.Pincus, *J. Chem. Phys.* 79, 997(1983).
- [132] J. S. Wang, K. Binder, *J. Chem. Phys.* 94, 8537(1991); G. G. Pereira, J. S. Wang, *J. Chem. Phys.* 105, 3849(1996); G. G. Pereira, J. S. Wang, *J. Chem. Phys.* 104, 5294(1996); G. G. Pereira, J. S. Wang, *Phys. Rev. E* 54, 3040(1996); G. G. Pereira, *J. Chem. Phys.* 106, 4282(1997); G. G. Pereira, *J. Chem. Phys.* 107, 3740(1997).
- [133] A. O. Parry, R. Evans, *J.Phys.A* 25, 275(1992).
- [134] A. O. Parry, R. Evans, *Physica A* 181, 250(1992).
- [135] A. O. Parry, J. C. Boulter, *Physica A* 218, 77 and 109(1995).
- [136] E. Brezin, B. I. Halperin, S. Leibler, *Phys. Rev. Lett.* 50, 1387(1983); R. Lipowski, D. M. Kroll, R. K. Zia, *Phys. Rev. B* 27, 4499(1983); D. S. Fisher, D. A. Huse, *Phys. Rev. B* 32, 247(1985).
- [137] K. Binder, D. P. Landau, A. M. Ferrenberg, *Phys.Rev. E* 51, 2823(1995); K. Binder, R. Evans, D. P. Landau, A. M. Ferrenberg, *Phys. Rev. E* 53, 5023(1996).
- [138] T. Kerle, J. Klein, K. Binder, *Phys. Rev. Lett.* 77, 1318(1996); T. Kerle, J. Klein, K. Binder, preprint, January 1998.
- [139] M. Sferrazza, C. Xiao, R. A. L. Jones, D. G. Bucknall, J. Webster, J. Penfold, *Phys. Rev. Lett.* 78, 3693(1997).
- [140] A. Werner *et al*, work in preparation.
- [141] L. L. Moseley, *Int. J. Mod. Phys. C* 8, 583 1997).
- [142] C. E. Scott, C. W. Macosko, *Polymer* 35, 5442 (1994); see also *Macromol.Symposia.:Polym. Blends* 112, 141-175(1996).
- [143] B. O'Shaughnessy, U. Sawhey, *Macromolecules* 29, 7230(1996); *Phys. Rev. Lett.* 76, 3444(1996).
- [144] S. T. Milner, G. H. Fredrickson, *Macromolecules* 29, 7386(1996); G. H. Fredrickson, *Phys. Rev. Lett.* 76, 3440(1996).
- [145] M. Müller, *Macromolecules* 30, 6353(1997).
- [146] R. Haswgawa, M. Doi, *Macromolecules* 30, 5490(1997).

- [147] K. S. Schweizer, M. Fuchs, G. Szamel, M. Guenza, H. Tang, *Macromol. Theory Simul.* **6**, 1037(1997).
- [148] M. Murat, K. Kremer, preprint, October 1997.